# A comprehensive review of hydrogen production and storage: A focus on the role of nanomaterials

**Citation for published version:**
Epelle, E, Desongu, K, Obande, W, Adeleke, A, Ikubanni, P, Okolie, J & Gunes, B 2022, 'A comprehensive review of hydrogen production and storage: A focus on the role of nanomaterials', *International journal of hydrogen energy*, vol. 47, no. 47, pp. 20398-20431. https://doi.org/10.1016/j.ijhydene.2022.04.227

**Digital Object Identifier (DOI):**
10.1016/j.ijhydene.2022.04.227

**Link:**
Link to publication record in Edinburgh Research Explorer

**Document Version:**
Peer reviewed version

**Published In:**
International journal of hydrogen energy

# A comprehensive review of hydrogen production and storage: A focus on the role of nanomaterials

Emmanuel I. Epelle[1], Kwaghtaver S. Desongu[2], Winifred Obande[3], Adekunle A. Adeleke[4], Peter P. Ikubanni[4], Jude A. Okolie[5], Burcu Gunes[6]

[1]School of Computing, Engineering and Physical Sciences, University of the West of Scotland, Paisley, United Kingdom.

[2]Department of Chemical Engineering, Federal University of Technology, Minna Nigeria.

[3]School of Engineering, Institute for Materials and Processes, The University of Edinburgh, Robert Stevenson Road, Edinburgh, EH9 3FB, Scotland, United Kingdom.

[4]Mechanical Engineering Department, Landmark University, Omu Aran, Nigeria

[5]Department of Chemical and Biological Engineering, University of Saskatchewan, Saskatoon, Saskatchewan, Canada.

[6]School of Biotechnology and DCU Water Institute, Dublin City University, Glasnevin, Dublin, Ireland

*** Corresponding author:**

Dr. Burcu Gunes

Assistant Professor in Bioprocess Engineering

School of Biotechnology

DCU Water Institute

Dublin City University

burcu.gunes@dcu.ie

## List of Abbreviation

| | |
|---|---|
| AC | Activated carbon |
| AER | Alkaline enhanced reforming |
| APR | Aqueous phase reforming |
| CCD | Central composite design |
| CMH | Complex metal hydrides |
| CMPs | Conjugated microporous polymers |
| CNT | Carbon nanotubes |
| CSHNSs | Core/shell heteronano structures |
| DFT | Density functional theory |
| DOE | US Department of Energy |
| ENME | Electrospun nanomaterials-based electrocatalysts |
| FT | Fischer-Tropsch |
| GDA | Generalized gradient approximation |
| GNP | Graphene nanoplatelets |
| HER | $H_2$ evolution reaction |
| HTF | Heat transfer fluid |
| IRMOF | Isorecticular metal-organic frameworks |
| LCPs | Linear conjugated polymers |
| LDA | Local density approximation |
| MHHSS | Metal hydride based $H_2$ storage system |
| MOF | Metal-organic framework |
| MWCNT | Multi-walled carbon nanotubes |
| OER | Oxygen evolution reaction |
| QCNs | Quantum Cu (II) nanodots |
| SMR | Steam reforming reaction |
| SWCNT | Single-walled carbon nanotube |
| TOF | Turnover frequency |
| WGSR | Water-gas-shift reaction |

# Abstract

Nanomaterials are beginning to play an essential role in addressing the challenges associated with hydrogen production and storage. The outstanding physicochemical properties of nanomaterials suggest their applications in almost all technological breakthroughs ranging from catalysis, metal-organic framework, complex hydrides, etc. This study outlines the applications of nanomaterials in hydrogen production (considering both thermochemical, biological, and water splitting methods) and storage. Recent advances in renewable hydrogen production methods are elucidated along with a comparison of different nanomaterials used to enhance renewable hydrogen production. Additionally, nanomaterials for solid-state hydrogen storage are reviewed. The characteristics of various nanomaterials for hydrogen storage are compared. Some nanomaterials discussed include carbon nanotubes, activated carbon, metal-doped carbon-based nanomaterials, metal-organic frameworks. Other materials such as complex hydrides and clathrates are outlined. Finally, future research perspectives related to the application of nanomaterials for hydrogen production and storage are discussed.

**Keywords**: Hydrogen; Nanomaterials; Electrolysis; Water splitting; Gasification, Activated carbon.

**Word count: 11360**

# 1. Introduction

Recently there has been a tremendous increase in the number of researchers, scholars, countries, and stakeholders considering hydrogen energy as a panacea for the increasing energy demand, environmental pollution, and overdependency on fossil fuels. More specifically, the world is facing greenhouse gas emissions, climate change, energy security, and water pollution challenges [1]. Therefore, developing alternative energy sources that are environmentally friendly and sustainable over a long duration is imperative.

Hydrogen is preferred as an energy carrier and a promising alternative to carbon-based fuels due to its renewability and pollution-free characteristics. It should be mentioned that hydrogen is pollution-free when combusted because it does not have $CO_2$. However, its renewability and "pollution-free" characteristics are based on the production routes. The combustion of $H_2$ of hydrogen releases water vapour, and its calorific value (141.9 kJ/g) is three times more than that of gasoline (47 kJ/g) and 2.6 times greater than natural gas (54 kJ/g) [2]. Compared with other fuels such as ethanol and natural gas, hydrogen is lighter with a density of 0.08988 g/L at standard temperature and pressure (STP) and a molar mass of 1.008 g/mole [3]. Moreover, the energy density per volume of hydrogen (0.09 $kg/m^3$) is relatively low at STP compared to other fuels.[3] Due to the low volumetric energy density, storing hydrogen in vehicles requires a large tank at a higher pressure than other gaseous fuels [4]. Therefore, it is imperative to develop advanced storage technologies to increase energy density per volume. The lightweight properties of hydrogen makes it a unique and versatile energy carrier with a broad spectrum of applications. Okolie et al. [5] recently summarized different industrial applications of hydrogen. Although hydrogen is a promising fuel, its production and storage are associated with several technical and scientific challenges that impede its worldwide implementation [6].

Steam reforming of natural gas (SMR) is a widespread hydrogen production method. However, Acar and Dincer's [6] studies reveal that fossil-based hydrogen production is one of the most environmentally harmful processes. As such, there is an urgent need to develop large-scale, cost-effective, renewable, and ecologically benign hydrogen production processes.

Another challenge, as noted earlier, is associated with the lack of practical, easy, safe and cheap storage methodologies [7]. Additionally, the onboard storage of hydrogen in vehicles is another bottleneck because of the stringent requirements in its storage. Currently, hydrogen is often stored in the gaseous or liquid form in pressurized or cryogenic tanks [8]. However, these technologies do not meet the requirements of large-scale storage. Therefore, there is a need to develop cost-effective, reliable, and safe storage systems to foster the development of a hydrogen economy.

Engineered nanomaterials have a size ranging from 1-100 nm and are produced and designed specifically to simulate their properties for specific applications. Nanomaterials are beginning to play a significant role in the development of new fields in addition to their tremendous impact on improving hydrogen production and storage [9].

Several studies have evaluated different areas where nanomaterials could improve hydrogen production and storage. Reddy et al. [9] reported recent research progress in the use of plasmonic photocatalyst nanoparticles for hydrogen production. Mao et al. [10] reviewed the application of different nanostructured materials for renewable hydrogen production, storage, and utilization. However, the review is solely focused on solar hydrogen production and does not consider renewable hydrogen from biomass conversion processes [10]. Recently, Abdalla et al. [11]outlined hydrogen production and storage challenges and prospects. However, recent advances on nano-based materials for hydrogen storage and production were lacking. This has partly motivated the work herein. To the best of the authors' knowledge, there is no comprehensive review that summarizes the advancement in the use of nanomaterials for hydrogen production and storage. Therefore, this study outlines the applications of nanomaterials in hydrogen production (considering both biological and water splitting methods) and storage. Other materials such as complex hydrides and clathrates used for hydrogen storage are also outlined in this study.

This review is organized as follows. The first section starts with the introduction, after which the methodology is briefly outlined. Different hydrogen production methods are comprehensively discussed in Section 3. The next section outlines various studies related to the application of nanomaterials for renewable hydrogen production with a focus on biological and thermochemical conversion processes. In Section 5, different hydrogen storage methods are discussed and compared. Section 6 reviews previous research on the application of various nanomaterials to facilitate hydrogen storage. The study ends with a conclusion and future perspectives.

## 2. Methodology

Google Scholar, Scopus, Web of Science, and PubMed were used as search engines for the initial search. The following keywords and/or phrases were used: complex metal hydrides, hydrogen storage nanomaterials, limitations of hydrogen storage, nanomaterials for renewable hydrogen storage, hydrogen storage nanoconfinement nanoelectrocatalysts, nanophotocatalysts, carbon nanotubes, catalytic nanomaterials, carbon-based nanocomposites, carbon cryogel nanocomposites, fullerene-based nanocomposites, and metal organic framework. The search was narrowed down to two categories. Category 1 is for articles published within the last eight years to ensure that the information presented is recent and relevant. The second category is for articles published in the 30 years to provide the readers with the research progress and pioneering findings in nanomaterials for hydrogen production and storage.

The articles were screened into two subcategories. In screening Category 1, studies related to the application of nanomaterials to renewable hydrogen production were considered. Category 2 focuses specifically on the applications of nanomaterials for hydrogen storage. Literature screening was performed by an initial reading of the articles' title, abstract, and conclusions to obtain the overall scope and objectives. Based on this, articles that fit the objectives of this study were selected. About 120 papers were chosen to fit the criteria.

## 3. Hydrogen production routes

Pure hydrogen hardly exists alone due to its high reactivity; instead, it is attached to carbon and oxygen in various compounds such as hydrocarbons, water, etc. A significant quantity of energy is needed to separate hydrogen from such compounds. Based on the separation methods, conversion processes, and the feedstock used for hydrogen production, colour codes such as green, grey, black, and blue are used, as shown in Fig.1. The hydrogen produced from natural gas via stream reforming without carbon capture and storage (CCS) is called grey hydrogen. Moreover, if bituminous or lignite coal is used as feedstock, the hydrogen is called black or brown hydrogen [12]. Steam reforming of natural gas coupled with CCS produces blue hydrogen. This type of hydrogen is carbon neutral if all the $CO_2$ is captured and stored underground. However, the process is termed "low carbon" if $CO_2$ is not captured completely. Hydrogen produced from electrolytic splitting using clean energy sources such as wind is green hydrogen [13]. Thermochemical and biological conversion processes also produce green hydrogen. Integrating biomass conversion processes with CCS produces even more greener hydrogen with negative $CO_2$ emissions.

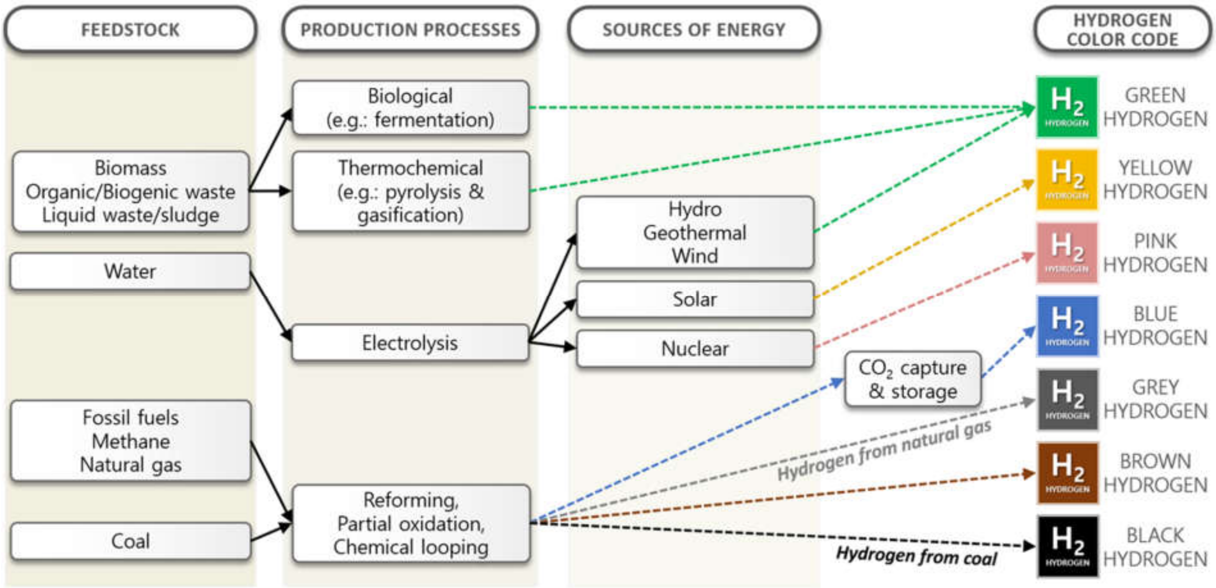

**Figure 1**: Hydrogen production routes and the associated colour codes (Note: the colour codes presented here are solely based on the present authors' perspectives and experiences, moreover naming convention and colour codes often differs across countries and over time.

## 3.1 Reforming reactions (steam, aqueous, alkaline enhanced, and autothermal reforming)

Steam reforming reaction (SMR) is the dominant process for large-scale hydrogen production, accounting for more than 59% of the global production from fossil fuels (natural gas, heavy oils/naphtha, and coal). The other common methods for hydrogen production from fossil fuels are alkaline enhanced reforming, aqueous reforming, and autothermal reforming [14].

SMR refers to the conversion of the hydrocarbons, usually methane and steam, into hydrogen and carbon dioxide at high temperatures (~800 °C) in the presence of a catalyst and under pressure (~3.5 MPa) (Equation 1). The CO present in the syngas also reacts with water to produce hydrogen and carbon dioxide through the water-gas-shift reaction (WGSR) (Equation 2) [15]. The produced gas mixture is then sent to sequential purification steps to achieve 100% hydrogen purity. To prevent catalyst poisoning, an additional desulphurization stage is required for high sulphur feedstocks before syngas generation [14]. Several metal catalysts such as Co, Ni, Rh, and Pt have been used to elevate hydrogen yield from steam reforming reactions [16,17].

$$CH_4 + H_2O \leftrightarrow CO + 3H_2 \qquad \Delta H = 206 kJ/mol \qquad (1)$$

$$CO + H_2O \leftrightarrow CO_2 + H_2 \qquad \Delta H = -41 kJ/mol \qquad (2)$$

Aqueous phase reforming (APR) of different types of oxygenated hydrocarbons such as glycerol, methanol, ethanol, or propanol is another route for hydrogen production. The process occurs in the presence of a metal catalyst at moderate temperature (225–265°C) and pressures (27–54 bar) [18]. Under these conditions, steam formation is inhibited, and the reaction would proceed in the aqueous phase. The APR produces high hydrogen yield and low CO yield due to its ability to thermodynamically promote WGSR [19]. APR process with biomass-based feedstock has been reported by several researchers [16,19,20]. A recent experimental study proposed a novel pathway that utilized the aqueous liquid from Fischer-Tropsch (FT) synthesis to produce biohydrogen through APR [21].

Alkaline enhanced reforming (AER) is another approach used to convert water-containing organics into hydrogen at low temperatures (<220 °C) and pressures in an alkaline medium (usually NaOH). The addition of an alkaline ensures that the reaction medium maintains a basic pH to create an environment that promotes conventional SMR [18]. The carbon produced from APR precipitates as solid $Na_2CO_3$ rather than gaseous pollutants (CO and $CO_2$) in SMR. Therefore, APR produces fewer greenhouse gases and is more environmentally friendly.

Partial oxidation, autothermal reforming, combined steam methane reforming with partial oxidation are also promising hydrogen production methods from hydrocarbons. During autothermal reforming, the hydrocarbon feed is partially oxidized in the presence of oxygen and steam to produce hydrogen-rich syngas [22].

## 3.2 Thermochemical Processes

Thermochemical processes for hydrogen production such as pyrolysis and gasification use heat and chemical reactions to decompose organic materials into hydrogen [23]. During pyrolysis, biomass is converted to bio-oil, char, tar, a mixture of $H_2$, CO, $CO_2$, and hydrocarbons in an oxygen-depleted environment at around 400 °C and 0.1-0.5 MPa [24]. Increased hydrogen production can be achieved by reforming the pyrolysis by-products such as aqueous liquid (bio-oil) or further conversion of the CO in the gaseous product to produce more hydrogen via WGSR. The pyrolysis gas mixture is purified, typically by a pressure swing adsorption or a $CO_2$ removal process [14]. Reaction temperature, residence time, and most importantly, the type of biomass and catalyst used in the process are the key factors affecting hydrogen yield during pyrolysis [25,26]. Based on these factors, pyrolysis can be classified as slow, fast, or flash, as detailed and compared in Table 1.

**Table 1:** Comparisons between different types of pyrolysis and hydrothermal liquefaction Nanda et al. [2], Okolie et al. [5]

| **Biomass conversion processes** | **Main products** | **Residence time (s)** | **Reaction temperature (ºC)** | **Biomass particle size (mm)** | **Heating rate (ºC/s)** |
|---|---|---|---|---|---|
| Fast pyrolysis | Biochar < Gases < Bio-oil | 0.5 – 10 | 400 – 800 | < 1 | 10 – 200 |
| Slow pyrolysis | Gases < Bio-oil <Biochar | 600 – 6000 | 300 – 700 | 5 – 50 | 0.1 – 1 |
| Flash pyrolysis | Biochar < Gases <Bio-oil | < 0.5 | 800 – 1000 | < 0.2 | 1000 |

Gasification is a thermochemical process that converts organic matter into hydrogen-rich syngas at high temperatures and can be either conventional or hydrothermal (also known as supercritical water gasification). Although both conventional and thermochemical gasification processes are comparable in terms of the desired product, they differ based on the composition of the gaseous products and the operating conditions. In conventional gasification, biomass is converted to syngas (mixture of $H_2$, CO, CO, $CH_4$, and other hydrocarbons), tar, and char in the presence of a gasifying agent like oxygen and/or steam. The process occurs at an operating temperature and pressure range of 500-1400 °C and 0-4 MPa, respectively [27]. The process yield is mainly dependent on the type of biomass, type of catalyst, particle size, steam-to-biomass ratio, and reaction temperature [28,29].

Hydrothermal gasification is the thermochemical conversion of organic materials into hydrogen-rich syngas under supercritical conditions (temperature > 374 ºC, pressure > 22.1 MPa) [30]. Water displays unique physicochemical properties such as gas-like viscosity and liquid-like density at supercritical conditions, leading to improved dissolution and mass transfer [31,32]. Despite being more advantageous in terms of improved hydrogen yield and the ability to handle wet feedstock without drying, hydrothermal gasification has several challenges limiting large-scale production. The high temperatures and pressures needed to attain supercritical conditions lead to an elevation in the operating cost compared with other biomass conversion technologies [23] and potential noise, explosion, injury, and odour risks [33,34].

## 3.3 Biological processes

Biological processes use microorganisms to decompose organic matter into hydrogen. Examples of such processes include biophotolysis and dark/photo fermentation. Biological hydrogen production processes have attracted global research interest owing to their applicability at ambient operating temperatures and pressures and waste recycling ability [35].

In direct biophotolysis, water undergoes prior splitting into hydrogen and oxygen ions by the photosynthetic activity of green algae. The hydrogen ions are then converted into $H_2$ (hydrogen gas) by the hydrogenase enzyme [36] under strictly anaerobic conditions ($O_2$ content <0.1%) due to the extreme enzyme sensitivity [37]. The major drawbacks of the biophotolysis process are complex bioreactor design with large surface areas for light capturing and low hydrogen conversion yields [36,38].

On the other hand, fermentative processes achieve simultaneous organic waste treatment and hydrogen production via microbial biomass transformation with or without oxygen [14]. In the metabolic process of dark fermentation, sequential carbon chain reactions are carried out by the obligate and facultative anaerobic bacteria to convert organic substrates into hydrogen, ethanol, and volatile fatty acids in the absence of light [36]. An initial pre-treatment step might be required to increase glucose digestibility when recalcitrant lignocellulosic biomass is used as a substrate [14]. For successful operations, pH should be maintained in a range of 5-6, and the produced hydrogen should constantly be removed from the system to stimulate the hydrogenase enzyme [37,38].

Photo-fermentation relies on the nitrogenase enzyme in photosynthetic bacteria to convert organic acids into $H_2$ and $CO_2$ [39]. In the case of using industrial wastewater as the substrate, an additional pre-treatment step is required for heavy metal and colour removal to attain sufficient light penetration [36]. Although photo-fermentation achieves higher theoretical $H_2$ production yields, the limited availability of organic acids, low efficiency in solar energy conversion, and complicated bioreactor demand with large surface areas are major limitations of this technology compared with dark fermentation [37,38]. Nonetheless, higher $H_2$ production yields with minimum solar energy dependency can be achieved by an integrated sequential dark/photo fermentation system with anaerobic and photogenetic bacteria.

## 3.4 Hydrogen production through water splitting

Water splitting involves water decomposition into $H_2$ and $O_2$ through a reaction involving charge carriers. This promising $H_2$ generation process has improved over time, and there are currently four distinct methods explored for this purpose; these include thermochemical (thermolysis), electrochemical (electrolysis), photochemical (photolysis), and photoelectrochemical methods [40]. These methods are still subjected to ongoing research and are at different levels of development. The thermolysis process is very similar to electrolysis except for the use of thermal energy for water splitting instead of electricity.

Thermochemical water splitting involves the decomposition of water into $O_2$ and $H_2$ through repetitive series of chemical reactions, usually at temperatures between 500–2000ºC [41]. In theory, heat is the only form of energy required for this reaction to occur, as every other resource is recycled and reused. As a result of the high heat energy requirement, the process is costly. Therefore, it has limited its application in the large-scale production of $H_2$, despite offering more than 77% efficiency [40,41]. During thermochemical water splitting, the water should be heated above 2500°C to achieve hydrogen separation [14]. Besides, several thermolysis cycles (Cu-Cl and Mg-Cl) are preferred to help lower the reaction temperature. In these cycles, sequential chemical reactions are carried out at different temperatures where the heat is converted into a chemical energy carrier in the form of $H_2$ [42,43].

Electrochemical water splitting involves splitting water into $H_2$ and $O_2$ by the passage of electrical energy in electrochemical cells. A typical electrolysis unit consists of an anode (negatively charged) and cathode (positively charged) probes submerged in an electrolyte. Following the passage of electric current, $H_2$ is produced in the cathode while $O_2$ accumulates around the anode [44]. The redox reaction, where two half-reactions occur simultaneously, is one of the most promising methods of renewable $H_2$ production. An oxidation half-reaction, commonly called oxygen evolution reaction (OER), occurs at the anode of the electrochemical cell. In contrast, a reduction half-reaction, commonly called $H_2$ evolution reaction (HER), occurs at the cathode of the electrochemical cell. The OER and HER are represented by Equations 3 and 4, respectively.

$$2H_2O \rightarrow O_2 + 4H^+ + 4e- \qquad (3)$$

$$2H^+ + 2e^- \rightarrow H_2 \tag{4}$$

Alkaline, proton exchange membrane, and solid oxide electrolysis cells are currently the most developed technologies for pure hydrogen production from water splitting. However, the electrochemical reactions are extremely endothermic, leading to high electricity consumption, rendering these technologies economically unfeasible [14].

The photolysis process is very similar to electrolysis; however, the energy requirement of the water splitting is provided by the absorbed sunlight by the semiconducting materials. An electron-hole pair is produced and separated due to the electric field between the electrolyte and semiconductor. The holes stay at the anode and decompose water into hydrogen ions ($H^+$) and oxygen. The $H^+$ travels to the cathode through the electrolyte, while the electrons travel through an external circuit to react with the $H^+$ at the cathode to produce $H_2$ [45].

Water splitting can also be caused by sunlight and electricity, in the presence of photocatalysts [46] absorbing sunlight to generate electrons and holes. The charges are separated and migrate to the catalyst's surface. After that, a surface reaction with the $H_2O$ molecules occurs, facilitating water splitting into $H_2$ and $O_2$ (redox). In most cases, photocatalysis requires a sacrificial (electron) donor that removes the photogenerated holes from the catalyst [40]. The sacrificial donors, which are primarily carbon-based molecules, get oxidized in the process to form $CO_2$. This has environmental implications and must be addressed to make the process more attractive. There is, therefore, a recommendation that the term "water splitting" should not be used when a sacrificial donor is involved [40]. In addition, there are also concerns about the low conversion efficiency, high cost of conversion, and unstable catalysts associated with photocatalytic water splitting [46]. These concerns indicate that there is substantial progress required before photocatalytic water splitting becomes a credible and sustainable alternative for hydrogen production.

Photoelectrochemical hydrogen production involves splitting water with sunlight and specialized semiconductors called photoelectrochemical materials [40]. The semiconductor materials are similar to those used in photovoltaic solar electricity generation. However, they are immersed in a water-based electrolyte in which sunlight facilitates the water-splitting process. The process is promising because it can produce cost-effective hydrogen with improved conversion efficiency. However, the current limitations are the semiconductor materials' durability, cost, and lifetime and low sunlight absorption [47]. Table 2 outlines the advantages and limitations of different hydrogen production methods discussed in this section.

**Table 2**: Major advantages and disadvantages of different hydrogen production technologies

| | **Advantages** | **Disadvantages** |
|---|---|---|
| Fossil Fuel Treatment<br>Steam reforming<br>Partial oxidation<br>Autothermal steam reforming | • Most established industrial process.<br>• Higher production yields.<br>• Economically more feasible.<br>• High purity hydrogen is produced. | • Causes massive GHG emissions and increased carbon footprint.<br>• Limited feedstock availability due to the depletion of fossil fuels.<br>• High operation temperature requirement<br>• Lack of adequate carbon capture storage technologies (CCS).<br>• Catalyst poisoning due to sulphur-containing feedstock. |
| Thermochemical Processes<br>Gasification<br>Pyrolysis | • Higher production yields than biological processes.<br>• $CO_2$ neutral<br>• Sustainable feedstock supply.<br>• Short hydraulic retention times.<br>• Negative $CO_2$ emission when CCS is used. | • High operation temperature requirement.<br>• Increased tar formation.<br>• Varying $H_2$ content based on biomass seasonality and impurities. |
| Biological Processes<br>Biophotolysis<br>Dark/photo fermentation | • Sustainable feedstock availability<br>• Negative $CO_2$ emission when CCS is used.<br>• More environmentally friendly than fossil fuel production routes and thermochemical processes<br>• Less energy-intensive due to mild operating conditions<br>• Provides $H_2$ production and waste treatment simultaneously (fermentation). | • Low production yields and rates<br>• Long hydraulic retention times requirement<br>• Difficulty in maintaining process stability<br>• High $O_2$ sensitivity<br>• Large surface area requirement for collecting adequate light (biophotolysis)<br>• No waste recycling (biophotolysis) |
| Water splitting<br>Electrolysis<br>Thermolysis<br>Photolysis<br>Photoelectrochemical | • Sustainable feedstock supply<br>• $O_2$ is the sole by-product<br>• $CO_2$ neutral | • High investment and operational costs<br>• Low conversion efficiency<br>• Corrosion problems<br>• Sunlight demand (photolysis) |

# 4. Nanomaterials for renewable hydrogen production

## 4.1 Nanoelectrocatalysts

The application of nanomaterials has gained popularity in electrochemical, photochemical, and photoelectrochemical water splitting. Electrocatalysts have a crucial role in facilitating water splitting to unlock its full potential of producing pure hydrogen that can meet the world's fast-growing energy demand. This is because the two half-reactions of water splitting – HER, and especially OER, are kinetically limited, requiring electrocatalysts to speed them up as well as to make them less energy-consuming [40].

Nanomaterials are taking centre stage in recent electrocatalytic and photocatalytic research because they exhibit desirable and tenable mechanical and electrical properties, offering large surface areas that significantly lower energy barriers and promote electron transfer at the electrodes. For instance, electrospun nanomaterials-based electrocatalysts (ENME) can undergo electronic modulation and interface engineering to enhance their catalytic performance [48]. Electronic modulation refers to catalyst doping with heteroatoms, while interface engineering is the construction of hybrids with unique interfaces that can contribute to more active sites on the catalysts.

Pt-group-metal-based electrocatalysts (Pt, Pd, Ru, Ir, and Rh) have proven to be excellent nanoelectrocatalysts for water splitting hydrogen production [49]. However, they are scarce, expensive, vulnerable to electrocatalysis poisoning, and tend to agglomerate [50], preventing their commercial application. Therefore, researchers are focusing on improving the catalytic efficiencies of non-noble metal-based electrocatalysts for water splitting-based hydrogen production since they are cheaper and more earthly abundant [50,51]. Some popular non-noble metal elements under study are Ni, Co, P, Fe, Cu, C, N, Se, W, Mo, and S. Table 3 shows some notable, recent findings of nanoelectrocatalysts for water splitting hydrogen production.

**Table 3:** Summary of some recent research contributions on nanoelectrocatalytic generation of $H_2$.

| **Reference** | **Approach** | **Overpotential** | **Current density** | **Tafel slope** | **Comments** |
|---|---|---|---|---|---|
| Kumar et al. [51] | Experimental assessment using Teflon-lined autoclave and centrifuge | 1.4 – 2.0 V | 1 – 10 mA cm$^{-2}$ | 134 and 152 mVdec$^{-1}$ (HER) | A multi-step solvothermal process was used to synthesize multi-shelled NiO/Ni/Graphene and $Co_3O_4$/Co/Graphene nano-spheres from MOFs, producing a highly efficient and stable catalyst for both HER and OER in acid media. The Co-based catalyst proved more efficient. |
| Narwade et al. [49] | Experimental assessment via morphological characterization (TGA, TEM, FESEM, EDAX, XRD) | 582 mV for HER in an acidic medium | 10 mA cm$^{-2}$ | 63 mVdec$^{-1}$ for HER in an acid medium; 41 mVdec$^{-1}$ for OER in basic media | A bifunctional, noble metal-free electrocatalyst was synthesized by a chemical process using Ni/NiO on reduced graphene oxide (Ni/NiO @ rGO). |
| Wang et al. [52] | An experimental study using HRTEM | 325-540 mV for OER and 337-404 mV for HER in an alkaline media. | 10 mA cm$^{-2}$ | 97-157 mVdec$^{-1}$ (HER); 65-162 mVdec$^{-1}$ (OER) | A promising, high-active and stable bifunctional electrocatalyst ($CeNiFeO_x$) was proposed using a facile one-pot combustion approach. A new height of 20% solubility of Ni/Fe in the ceria lattices was achieved for the first time. $Ce_{0.8}Ni_{0.15}Fe_{0.05}O_x$ showed more excellent bifunctional catalytic performance. |
| Wan et al. [53] | Experimental assessment via electrostatic spinning and characterization | 133 mV for HER in an acidic medium | 10 mA cm$^{-2}$ | — | $CoSe_2$ nanostructured particles were synthesized on 3D nano-netlike carbon fibres ($CoSe_2$-CFN) by a spinning technique. The $CoSe_2$-CFN is characterized by high CoSe2 particle dispersion, high electrical conductivity, and catalytic activity. |
| Han et al. [54] | An experimental study via FE-SEM, EDS, TEM and XRD) | 290 for OER and 77 mV for HER, in alkaline media. | 10 mA cm$^{-2}$ | 56 mVdec$^{-1}$ | Cobalt phosphide incorporated with Vanadium (CoVP) self-supported catalyst on carbon cloth (CoVP@CC) was proposed in the study as a highly efficient, bifunctional electrocatalyst for OER and HER in alkaline medium. |
| Jadhav et al. [55] | Experimental study using electrosynthesis. | 240 and 401 mV for OER and HER. | 100 mA cm$^{-2}$ | 189 mVdec$^{-1}$ (OER); 103 | This study fabricated an organic-inorganic nanohybrid, namely BSeF/$Ni(OH)_2$, using one-step reductive electrosynthesis. The synthesized BSeF/$Ni(OH)_2$ was |

| | | | | | |
|---|---|---|---|---|---|
| | | | | mVdec$^{-1}$ (HER) | demonstrated to be a bifunctional electrocatalyst with an excellent performance: |
| Yan et al. [56] | Experimental and theoretical study using VASP (Viena *ab initio* Simulation Package) | 67mV (HER) in acidic media and 89 mV (HER) in basic media. | 10 and 100 mA cm$^{-2}$ | 57 mVdec$^{-1}$ and 82 mVdec$^{-1}$ in acidic and basic media. | A self-supported, hierarchical, and edge-rich electrocatalyst from nickel phosphide nanosheets arrays on nickel foam ($Ni_2P$ NSs) showed highly efficient catalytic ability for HER in both acidic and basic media. |
| Dai et al. [57] | Experimental / Density Functional Theory (DFT) | 171 and 243 mV for HER and OER, respectively | 10 mA cm$^{-2}$ | 28.1 mVdec$^{-1}$ | A new bifunctional electrocatalyst for water splitting was found in $CoNi_2S_4/Ni_3S_2$ on nickel foam ($CoNi_2S_4/Ni_3S_2$@NF) in alkaline media. The obtained electropotentials supersede those of metallic NF and $Ni_3S_2$ separately. DFT calculations showed that the strong coupling between $CoNi_2S_4$ and $Ni_3S_2$ improves the electrochemical performance. |
| Kumar and Bhattacharyya. [58] | Experimental assessment applying thermal treatment in air. | 271 and 197 mV for OER and HER in alkaline medium | 10 mA cm$^{-2}$ | 48 mVdec$^{-1}$ (OER); 130 mVdec$^{-1}$ (HER) | A bifunctional electrocatalyst for efficient water splitting was manufactured from porous NiFe-oxide nanocubes (NiFe-NC). It also shows corrosion-resistant properties for water splitting, in addition to its long-term stability. |
| Zeng et al. [59] | Experimental in combination with DFT | 80 and 210 mV for HER and OER, respectively | 10 mA cm$^{-2}$ | 65 mVdec$^{-1}$ (HER); 62 mVdec$^{-1}$ (OER); | A nanoelectrocatalyst was produced through a formation of a 3D-heterogeneous-nickel phosphide and its sulphide ($Ni_2P$ and $Ni_3S_2$) on nickel foam ($Ni_2P/Ni_3S_2$@NF), which enhances its catalytic performance for water splitting in alkaline media. |
| Mugheri et al. [60] | Experimental study on a solarton potentiostat | 0.31 V | 10 mA cm$^{-2}$ | 42 mVdec$^{-1}$ | Pristine SnCo and Cu-doped SnCo nanoelectrocatalysts were synthesized and studied. Cu-doped with 46% Cu showed an excellent HER catalytic performance comparable to the precious Pt/C. |
| Wang et al. [61] | Experimental in a Teflon-lined stainless-steel autoclave) | 117 mV for HER | 10 mA cm$^{-2}$ | 66 mV dec$^{-1}$ | $MoSe_2$@$Ni_{8.85}Se$ electrocatalyst was shown to have excellent conductivity and abundant exposed sites that greatly improved HER in an alkaline medium. |

Some key parameters that can be used to measure and compare nanoelectrocatalysts performances include, but are not limited to: overpotential values (mV), Tafel slopes ($mVdec^{-1}$), turnover frequency (TOF), binding energy for reaction intermediates, adsorption free energy (eV), Faradaic efficiencies (%), electrochemical surface area ($cm^2$), stability time with unchanging overpotential, mass activity ($mAmg^{-1}$), specific activity ($mAcm^{-1}$), charge transfer resistance (ohm), disruption of electronic, electron density at the Fermi level. It is also important that suitable nanoelectrocatalysts are bifunctional, environmentally friendly, and inexpensive to minimize hydrogen production costs by water splitting while maintaining a safe environment. Currently, no single catalyst possesses all the characteristics mentioned above [48,50,62].

While electrocatalysts and photocatalysts are both applied to catalyze water-splitting reactions for hydrogen production, they have notable differences in properties [63]. Electrocatalysts utilize externally induced electrical energy, and photocatalysts use solar energy. Qian et al. [63] highlighted the superior performance of electrocatalysts compared to photocatalysts and other differences between them. Nonetheless, this review expounds on the performance of a wide range of electrocatalysts for $H_2$ production based on recent research contributions, as shown in Table 3. Subsequently, it presents a detailed review of photocatalysts for $H_2$ production in Section 4.2.

## 4.2 Nanophotocatalysts

Generally, photocatalytic $H_2$ generation can be attained via photo splitting of water or photo reforming of organic species [64,65]. These processes usually require catalysts capable of absorbing radiation in the visible range and exciting electrons to the energy level needed for $H_2$ production [64]. Some nanomaterials, which are currently used for the photocatalytic production of $H_2$ include SiC, $TiO_2$, CdS, and $CuInSe_2$, which can be generally categorized into metal-oxide (such as $TiO_2$ and $WO_2$) and non-metal oxide (such as g-$C_3N_4$, $B_4C$, $CuInSe_2$, and CdS) photocatalysts [66]. The current attainable $H_2$ productions efficiencies (solar-to-fuel) using these photocatalysts are low and far from meeting the required operational requirements for industrial applications [64].

Research advancements in the field of photocatalytic water splitting have led to the development of more than 100 new catalysts, including carbides, sulphides, and oxides [67]. Despite these advancements, several challenges affecting their industrial applicability still exist. Some of these include the selective activeness of photocatalysts to ultraviolet light (low visible-light quantum efficiency), rapid recombination of photogenerated charges, poor durability and physicochemical stability, high toxicity, and difficulty in preparing the catalyst on a large scale [68–70]. The factors affecting the performance of nanophotocatalysts for water splitting are outlined in Table 4.

**Table 4:** Factors affecting nanophotocatalyst performance and selection Bhatt and Lee. [66], Ganguly et al. [70].

| **Factors based on photocatalyst conversion efficiency** | **Factors based on practical application & operating conditions of the photocatalytic process** |
|---|---|
| Extent of light absorption (specific photoactivity > $10^4$ µmoles $H_2$/h.g – | Resistance and stability under visible light (photohydrostability without undergoing photocorrosion in aqueous solution). |
| Bandgap and exciton generation/charge mobility. | Nature of co-catalyst and preparation method. |
| Ability to promote H-O bond cleavage via a reduction of the reaction energy barrier (500 kJ/mol). | pH and operating temperature. |
| The extent of separation and recombination of photogenerated holes and electrons (charge carriers). | Size and shape tunability of photocatalyst particles, including morphology/structure and crystallinity. |
| Charge collection rate at electrodes. | The concentration of sacrificial agent (photoreforming). |
| Specific area (1D or 2D nanostructure) | Cost-effectiveness |
| The removal of nanoarchitectures by photons so that they reach the reactive site | Toxicity level |
| Suitability of sacrificial electron donor | Suitability for large scale preparation |

Poor light absorption and insufficient charge separation are the main reported factors; these are, in turn, a consequence of large bandgaps of the photocatalysts [71,72]. These large band gaps (mainly associated with metal oxides) often lie outside the visible light region in the electromagnetic spectrum [66]. Hence, they are incapable of utilizing the solar spectrum, regardless of their highly active catalytic properties (photocatalysts, which are active under visible light, are more efficient and effective because visible light constitutes a significant portion of electromagnetic radiations)

[71]. For instance, $TiO_2$ (with a bandgap of 3.2 eV) is limited to a solar-to-$H_2$ conversion efficiency of 1%, whereas $Fe_2O_3$ (with a 2.2 eV bandgap) has a theoretical efficiency of 15% [66,73].

Some of the popular photocatalysts include a group of materials known as graphitic carbon nitrides, conjugated microporous polymers (CMPs), linear conjugated polymers (LCPs), and covalent organic frameworks [69,71,74]. Among these photocatalysts, graphitic nitrides (g-$C_3N_4$), which belong to the class of organic semiconductors) have been widely studied. They have emerged as viable candidates for solar-driven $H_2$ production via water splitting [75]. This may be attributed to their optoelectronic properties and reduced environmental footprints compared to inorganic and metal-complex materials. However, their inherent large molecular structures often yield bulky particles in water, which are higher than the penetration length scale of light [69]. The inevitable effect of this bulkiness is significantly optical losses, which ultimately reduce the catalytic performance. Thus, the particle size of the photocatalyst is a predominant factor affecting the catalyst's performance.

The size reduction of the particles to a few tens of nanometres can enhance their photocatalytic performance [76]. Enhancing photocatalytic performance can be done using specialized methods like nano-structure engineering to achieve thin layer nanosheets from bulk g-$C_3N_4$ [68,71]. Some of the methods include physical exfoliation (liquid and chemical), emulsion polymerization, sonification, template synthesis, and nanoprecipitation of polymer dots. Further details of these methods are provided by Mahzoon et al. [68]. Moreover, the anisotropic 1D nanostructures have been adopted in several studies due to the different behaviours of charge carriers obtained in different directions. One dimensional hierarchical structure comprising of $Ni_3S_2$ nanosheets grown on a carbon nanotube backbone was constructed by Zhu et al. [77]. Remarkably, this hybrid 1D hierarchical structure showed significantly enhanced photocatalytic activity in $H_2$ production from water splitting. Similarly, the work of Chava et al. [78] featured the development of 1D CdS–Au/MoS2 hierarchical core/shell heteronano structures (CSHNSs) by a facile two-step hydrothermal method; high stability and efficiency toward hydrogens production were observed with this nanophotocatalyst.

2D nanostructures, on the other hand, are desirable because they provide numerous reaction sites due to their increased specific area. Their short diffusion length reduces the probability of recombination of photoexcited charge carriers compared to the bulk forms of the photocatalysts

[68]. Ganguly et al. [70] provide a detailed review with emphasis on 2D nanomaterials for photocatalytic $H_2$ production. Zhang et al. [79] formulated a 2D nanophotocalyst by doping ultrathin nanosheets of $TiO_2$ with quantum Cu(II) nanodots (QCNs). Their analysis further demonstrated that suppressing the recombination rate of the photogenerated electron-hole pair enhances the materials' photocatalytic performance. Xu et al. [80] showed that the photocatalytic activity of g-$C_3N_4$ nanosheets was improved by 13-fold after electrostatically assembling it with hematite α-$Fe_2O_3$ nanoplates. Pt was applied as a co-catalyst, whereas triethanolamine was utilized as a hole scavenger. A cost-effective and straightforward method for fabricating a hybrid 1D-2Dg-$C_3N_4$ heterojunction nanophotocatalyst has been proposed by Mahsoon et al. [68]. At present, modifications via co-catalysts for performance improvement, as shown in Fig. 2, have been exploited to enhance the catalytic performance [81].

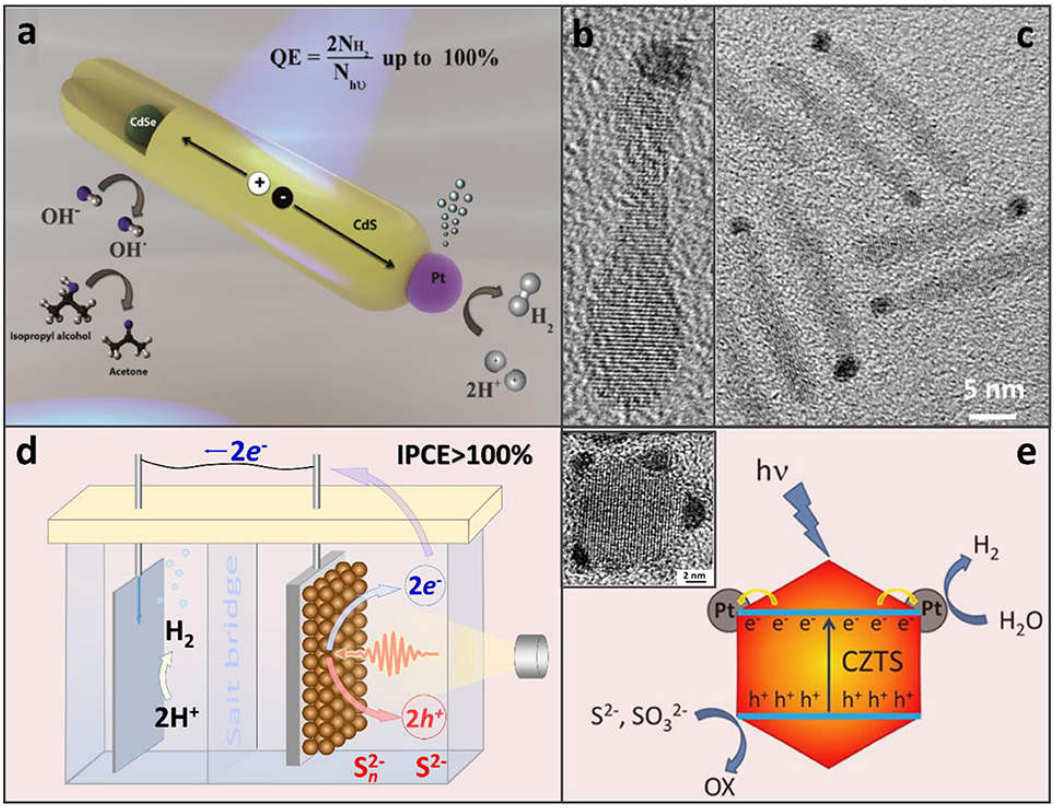

**Figure 2**: (a) Pt co-catalyst appended to CdSe/CdS nanorods; (b,c) TEM images of CdSE/CdS nanorods showing Pt co-catalyst on one side; (d) Photocatalytic/photoelectrochemical $H_2$ evolution for aqueous $Na_2S$ solution; (e) $H_2$ evolution on CZTS-Pt nanoparticles. Adapted from Xu et al. [80], Khon et al. [82], Kalisman et al. [83], Moroz et al. [84], respectively.

Morphology adjustments, band edge repositioning, and surface structure alterations have also been a subject of immense interest using these co-catalysts [66,85]. Their application may be carried out in several forms, such as ion doping, noble metal doping, metal-ion implantation, and sensitization [67,70]. Pt is the best noble metal for this purpose; however, its very high cost has led to the application of alternative cheaper noble metals such as Ag, Ni, Ru, Cu, Pd, and Ir [67]. Sensitization, a promising strategy, involves using a sensitizer (nanosized-metal particles). The sensitizer harvests sunlight (thus promoting visible light absorption), and thereafter, injects electrons into the conduction band of the main photocatalyst –a process referred to as plasmon-induced resonance energy transfer [64]. Furthermore, the tunable optical properties of semiconductor polymer photocatalysts (usually achieved by altering the polymer building blocks) has also gained research attention; poly(p-phenylene), poly(azomethine)s, polybenzothiadiazoles, covalent organic frameworks, and microporous organic nanorods have been applied for photocatalytic $H_2$ production [86]. Better light-harvesting efficiency may be attained with these polymers when used with g-$C_3N_4$ compared to g-$C_3N_4$ alone [62].

Inorganic co-catalysts such as Ni-P have also been applied with pristine g-$C_3$-$N_4$ to enhance their photocatalytic activity [87]. The importance of this doping strategy has been effectively demonstrated in the work of Kalisman et al. [83], where a record 100% photon to $H_2$ conversion efficiency was attained using Pt-tipped CDSe@CdS nanophotocatalysts. However, the photochemical instability of CdS and the high cost of Pt are the main limitations of this strategy [83].

The application of metal oxide co-catalysts, which can act as photocatalysts themselves, has also been demonstrated by Zada et al. [71]. $SnO_2$ as a metal oxide has an outstanding UV response, although with a bandgap of 3.5eV. Its modifiable optical properties and exceptional stability make it suitable for photocatalysis. The authors showed that the heterojunctional combination with g-$C_3N_4$ with $SnO_2$ enhances charge separation for increased photocatalysis in comparison to g-$C_3N_4$ alone. For photocatalytic water splitting, Clarizia et al. [64] recommended that an efficient photocatalyst should have a bandgap greater than 1.6–1.8 eV and should be narrower than 2.2eV to allow efficient activation under natural solar irradiation. Fig.3 shows the required energy for both solar driving and reforming photocatalytic reactions.

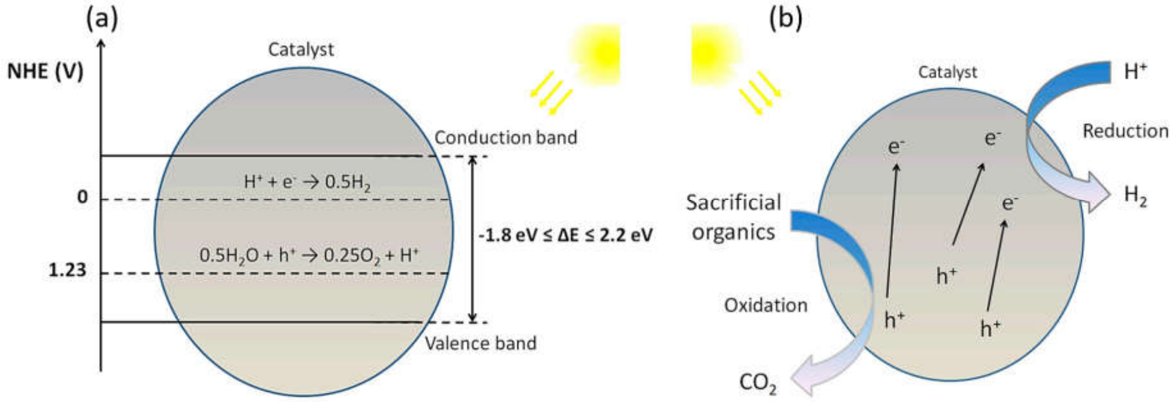

**Figure 3:** (a) Required energy gap for solar-driven photocatalytic water splitting and (b) photocatalytic reforming of organic species. Reprinted from Clarizia et al. [64].

Since photocatalytic reforming relies on the oxidation of organic sacrificial agents by photogenerated holes (which are in turn reduced by photogenerated electrons to form $H_2$ gas), it is required that the valence band be more positive than the redox potential of the sacrificial species, for efficient $H_2$ production [64]. Photoreforming of organics yields $H_2$ generation rates, which are more than 2 orders of magnitude higher than that of photocatalytic water splitting [88]. Hence, there is a need for an optimal selection of a sacrificial agent for these reactions. Further details of this photoreforming process can be found in the study of Clarizia et al. [64].

Biological systems, which are naturally nanoscaled, have also been employed as reliable platforms for engineering nanophotocatalysts. Photoelectrochemical analysis on $TiO_2$ catalyst shows effective charge transfer between a biological protein (bacteriorhodopsin) and $TiO_2$ nanoparticles and a consequent enhancement of photocatalytic ability (up to 5275 μmole of $H_2$ (μmole protein$^{-1}$h$^{-1}$) [72].

The discussion presented thus far demonstrates that a majority of the research efforts on the use of nanophotocatalysts for $H_2$ production have been mainly studied via experiments. Very few studies focusing on the application of theoretical/computational methods exist. These computational-based studies on nanophotocatalytic materials have mainly applied density functional theory (DFT) to predict ground-state properties as a function of the electronic density, primarily using $TiO_2$ photocatalysts. However, significant underestimations of the bandgap have been reported in many DFT-based studies [66]. The parameter is computed using the Kohn-Sham methods (via the generalized gradient approximation (GDA) or the local density approximation (LDA).

Nonetheless, using hybrid approaches, which utilized approximate DFT functionals (such as LDA) with the exact Hartree-Fock method, can potentially improve computational accuracy. A summary of some modelling-based studies in this regard is presented in Table 5.

**Table 5:** Summary of some recent research contributions on nanophotocatalytic generation of $H_2$.

| **Reference** | **Approach** | **Band gap information** | **Comments** |
|---|---|---|---|
| Yu et al. [69] | Combination of hydrophilic polymers with a nanoprecipitation technique | —<br>*However, a HOMO-LUMO gap is provided* | By applying a facile approach for the synthesis of nanoparticulate organic photocatalysts, a 70-fold improvement in the $H_2$ evolution rate was obtained (37.2 $mmol.h^{-1}.g^{-1}$) under sunlight irradiation. |
| Anthony Raja and Preethi. [89] | Experimental evaluation using a novel trapezoidal photoreactor | Reduction from 2.5 eV to 2.32 eV after CNT doping | Using synthesized CNT doped $CdZnS/Fe_2O_3$ nano-photocatalyst, a $H_2$ production rate of 2,679 µmol/h was obtained compared to $CdZnS/Fe_2O_3$ only (2,009 µmol/h). |
| Zada et al. [71] | Robust experimental catalyst characterization | 2.7 eV ($g\text{-}C_3N_4$) and 3.5 eV ($SnO_2$) | $g\text{-}C_3N_4$ nanosheets were constructed and functionalized with $SnO_2$ nanoparticles for $H_2$ production from water splitting. The hybrid catalyst fabrication ($g\text{-}C_3N_4$ – $SnO_2$) enhanced $H_2$ production compared to the individual application of $g\text{-}C_3N_4$ and $SnO_2$. |
| Mahzoon et al. [68] | Novel synthesis method for ($C_3N_4$(1D-2D)) catalyst | 2.70 ($C_3N_4$(1D))<br>2.84 ($C_3N_4$(2D))<br>2,78 ($C_3N_4$(1D-2D)) | A method for the fabrication of 1D-2D $g\text{-}C_3N_4$ heterojunction nanophotocatalyst was developed, which exhibited enhanced activity under visible light irradiation for $H_2$ production (2.6 and 4.1 times that of $C_3N_4$(1D) and $C_3N_4$(2D), respectively). |
| Maghrabi et al. [90] | Simplex centroid design (SCD) and Box–Behnken design (BBD) | 2.33 eV | Statistical optimal design of experiments was applied to fabricate a photocatalyst via optimal combinatorial ratios of a-$MoO_3$, $WO_3$ and CdS catalysts. The produced catalyst showed high potential for $H_2$ production from wastewater under a broad range of wavelengths. |
| Pati et al. [86] | Nanoprecipitation of polymer Pdots coupled with DFT validation | 2.38 eV, 1.98 eV, and 2.46 eV for Pdots 1, 2 and 3, respectively | Converting an organic polymer into polymer nanoparticles via nanoprecipitation is an efficient way of significantly improving photocatalytic performance. An $H_2$ evolution rate of up to 50 $mmol.g^{-1}h^{-1}$ is achieved. N in the benzothiadiazole unit is the main reactive site. |
| Pavliuk et al. [81] | Experimental assessment using a photocatalytic reactor | — | A nano-hybrid assembly is produced by combining natural product stabilized Ag nanoparticles, $TiO_2$, and Ru nanoparticles as a co-catalyst. A solar-to-fuel efficiency of up to 20% was achieved compared to 10-12% efficiencies obtainable in conventional photovoltaic electrolysis. |

| | | | |
|---|---|---|---|
| Balasubramanian et al. [72] | $H_2$ evolution measurements in a sealed reaction vessel | — | A light-harvesting biological proton pump (bacteriorhodopsin) was applied to enhance the visible light reactivity of $TiO_2$ photocatalysts for photon reduction (to $H_2$) using a Pt nanocrystalline catalyst. |
| Kaur and Singh. [91] | DFT calculations: 72-, 96- and 216-atom models utilized for amorphous $TiO_2$ representation | 2.85 eV, 2,85 eV & 2.7 eV for the 72-, 96- and 216-atom models | The electronic properties of amorphous and crystalline $TiO_2$ for photocatalytic $H_2$ production were compared. Amorphous $TiO_2$ may be utilized as a cheaper, more abundant, but slightly less efficient photocatalyst than $TiO_2$ in crystalline form. |
| Hanaor et al. [92] | Theoretical assessment using DFT | 3 meV difference between the rutile and anatase phase | Cationic doping of $TiO_2$ stabilizes the anatase phase relative to the rutile phase at standard conditions; anionic doping similarly inhibits anatase to rutile transformations. The effects of the tested dopants on the stability of the anatase phase are shown to be in the order: F>Si>Fe>Al |
| Das et al. [93] | Experimental assessment coupled with first-principles DFT calculations | — | The existence of charge transfer between graphene and deposited semiconductor and magnetic nanoparticles ($TiO_2$, ZnO, $Fe_3O_4$, Ni) was established. The possibility of tailoring the optoelectronic properties of graphene for $H_2$ production was demonstrated. |
| Kanda et al. [94] | Experimental characterization of a metal chalcogenide. | Bulk value of 1.75 eV | A green and straightforward photodeposition technique was utilized for the coupling of $MoS_2$ nanocrystals and $MoO_3$ molecules with $TiO_2$. In HCOOH aqueous solutions, high photocatalytic activity of the $MoS_2/TiO_2$ system is observed for $H_2$ generation. |

## 4.3 Nanomaterials for biological hydrogen production

Nanomaterials can be applied at different stages of biohydrogen production, including biomass pre-treatment, improved sugar and enzymes production, and enzymatic hydrolysis (Fig.4) [95].

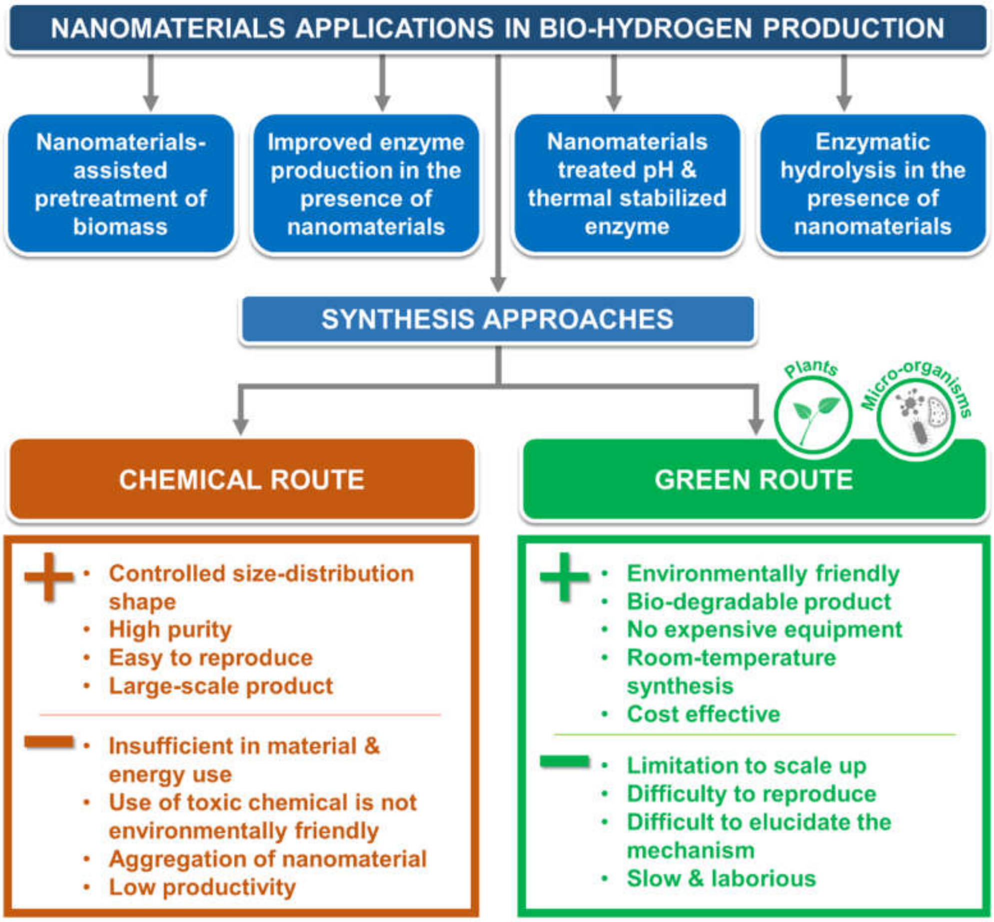

**Figure 4:** Application of nanomaterials at different stages of biological hydrogen production.

Nanomaterials such as Ni, Fe, and Cu play a significant role in improving biomass-to-biohydrogen processes. Fe and Ni behave like a cofactor on the active site of nitrogenase and hydrogenase enzymes, thereby elevating biohydrogen production yield [96]. They could also act as oxygen scavengers during fermentation by removing all the undesired oxygen present and minimizing the oxidation-reduction potential [95]. The removal of oxygen during fermentation creates a favourable anaerobic environment for the action of the hydrogenase enzyme and improves biohydrogen yield [97].

Previous studies also indicate that the addition of magnetic nanoparticles could influence the thermal stability and pH of cellulase enzymes and reduce the lag phase of microorganisms leading to improved hydrolysis [98]. In addition, the incorporation of magnetic nanoparticles (specifically Fe and Ni) to the bioreactor can enhance hydrogen yield because of their ability to bond to the active sites of the enzymes [99].

During dark fermentation, the hydrogenase enzymes are employed in breaking down sugar-rich organic substrates in the absence of oxygen. Although dark fermentation produces improved hydrogen yield, a low production rate is often observed [98]. Nanomaterials can create anoxic conditions, permitting fast $e^-$ transfer from $e^-$ donors to the corresponding $e^-$ acceptors, improving reaction kinetics and biohydrogen yield [100].

Engliman et al. [101] showed that the addition of Fe and Ni as metallic co-factors at the enzyme active sites during fermentative hydrogen production could act as a biocatalyst towards improving biohydrogen yield. The addition of Iron (II) oxide and nickel oxide under thermophilic conditions of 60°C led to an increase in hydrogen yield by 34.38% and 5.47%, respectively, compared to the control test [101]. Moreover, the microbes did not consume the metal nanoparticles at the end of the experiments. Wang et al. [102] studied the effect of nickel nanomaterial addition on biohydrogen production from dark fermentation. Optimal hydrogen production and biohydrogen yield of 288.6 ml and 296.1 ml per g glucose consumed, respectively, were reported at 5 °C and pH of 7.0 [102]. Taherdanak et al., [97]. used the central composite design (CCD) to study the effect of Fe and Ni nanoparticles on biohydrogen production from dark fermentation. The addition of both nanomaterials elevated the biohydrogen yield up to 200% higher than those in the corresponding control test [97]. Studies have shown that nanomaterials have the potential to modify the morphology of the microorganisms during dark fermentation in such a way that it could lead to improved biohydrogen yield [103].

Nanomaterials could also be impactful in elevating the hydrogen yield of photo-fermentation [104]. The nitrogenase enzymes used during photo-fermentation are dominated by Fe acting as a major co-factor at the enzyme's active site [99]. Besides, the inclusion of Fe and Ni during photo-fermentation helps maintain the enzymes' structural integrity. Moreover, photocatalytic nanomaterials such as ZnO and $TiO_2$ can improve the photo-conversion efficiency of the bacteria while supplying the required energy for hydrogen production [104]. The use of nanomaterials during photo-fermentation also results in the fast transfer of a photo-induced electron to the enzyme system, thereby improving the yield and productivity of hydrogen [104].

## 4.4 Nanomaterials for thermochemical hydrogen production

Nanomaterials are often used as active metals of heterogeneous catalysts or promoters during thermochemical processes [105]. Specifically, Ni-based catalysts are promising for hydrothermal gasification due to their small active metallic particle size, high dispersion rate, and effective catalytic activity [106]. Other nanocatalysts used for thermochemical hydrogen production via gasification include Fe, Cu, Pt, Ru, and Mg. The Ni nanocatalysts are preferred due to their low cost and effective hydrogen selectivity in hydrothermal conditions. Magnetic nanoparticles for thermochemical $H_2$ production can be classified as metal oxides, alloys, active metals, and ferrites, as shown in Fig.5 [107].

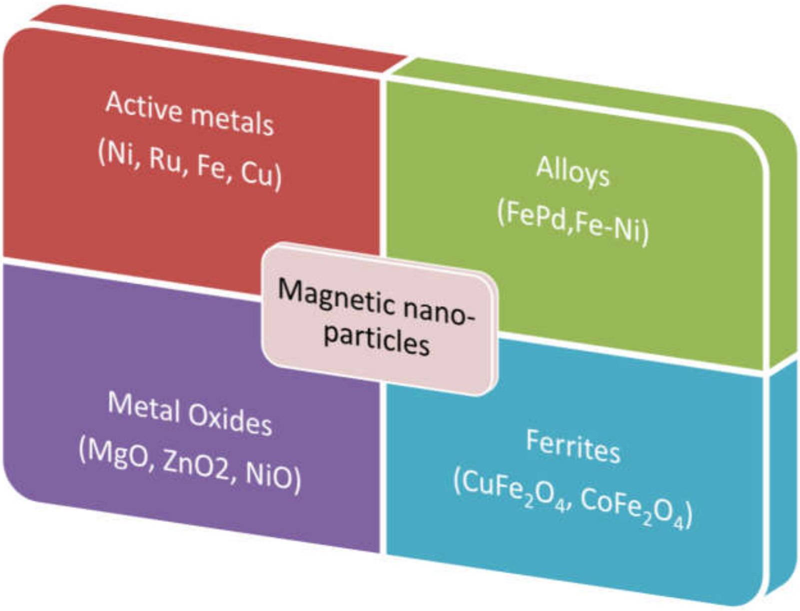

**Figure 5:** Classification of different nanoparticles used as catalysts for thermochemical conversion processes.

Fe–Ni supported on $\gamma$-$Al_2O_3$ showed improved catalysts ability during the gasification of algae under hydrothermal conditions [106]. Zn nanoparticles were used as a promoter for Ru/$\gamma$-$Al_2O_3$, to improve $H_2$ yield during the hydrothermal gasification of bagasse. The addition of Zn nanoparticles led to an elevation in the $H_2$ and total gas yield by 16.67% and 6.6%, respectively

[108]. Similarly, the addition of Cu promoter to Ni/CNT increased $H_2$ yield by a factor of 5.84 during the hydrothermal gasification of bagasse [109].

Metal oxide catalysts for thermochemical hydrogen production have been subjects of interest among several researchers because of their stability, low price, and regeneration ability when compared to transition metals catalysts [110]. Furthermore, the transition metal catalysts are prone to sintering, agglomeration, and deactivation due to the harsh SCW conditions and not being cost-efficient at large-scale applications. Metal oxides are easy to store, and transport and are more stable than metal catalysts [111]. Different metal oxide catalysts that have been used for thermochemical hydrogen production include $WO_3$, $TiO_2$, MgO, $ZrO_2$, ZnO, and NiO [111]. $WO_3$, $TiO_2$, and $ZrO_2$ are effective in elevating the gasification efficiency of glucose under hydrothermal conditions [111]. $ZrO_2$ and $TiO_2$ are widely known as thermally stable solid catalysts because of their ability to prevent methanation reactions while promoting hydrogen production [110].

Nanoparticles, specifically Ni and Fe, can also be directly impregnated into biomass pores before thermochemical conversion processes to eliminate the need for external heterogeneous catalysts [112]. This technique showed promising hydrogen yield and gasification efficiency [112,113].

## 5. Hydrogen storage methods

As the efforts to maximize the potential of $H_2$ as a clean and efficient energy source intensify, its efficient, safe and economical storage is critical for a thriving $H_2$ economy [114]. As a result of this realization, $H_2$ storage technologies have gained the attention of researchers over time [11,115,116]. Principally, $H_2$ is usually stored in four forms: compressed gas, liquefaction (cryogenic), cryo-compressed, and solid-state storage. These various methods of storage are at different stages of development. They have their strengths and weaknesses, making them apt for various applications, as discussed in the following sections and summarized in Table 6.

**Table 6:** Pros and cons of different $H_2$ storage methods.

| **Hydrogen storage methods** | **Advantages** | **Limitations** | **References** |
|---|---|---|---|
| **Compressed gas** | • Technology is matured and presently the best-understood method.<br>• For underground storage, it is safer, saves space and can be stored for a long time<br>• Lighter storage vessels are being developed.<br>• $H_2$ is stored in its natural form and can be directly used when needed | • Gravimetrically and volumetrically inefficient (low storage density)<br>• High energy cost required to compress the gas<br>• Large Storage vessels are required, leading to high space consumption, except in geological storage of compressed gas where gases are stored underground<br>• Not suitable for long term storage (due to high pressure) except for geological storage<br>• It is considered unsafe, as leakage may result in massive explosions | Durbin and Malardier-Jugroot. [118] Peschel. [119] |
| **Liquefaction** | • Gravimetrically and volumetrically efficient (high storage density).<br>• Technology is matured, hence developed.<br>• Relatively smaller storage vessels are required.<br>• Safer compared to compressed gas storage. | • High energy is required for liquefaction.<br>• Relatively high cost, mainly if carried out on a small scale.<br>• Storage vessels are expensive and consume land space (relatively less than compression vessels). | Durbin and Malardier-Jugroot. [118] Peschel. [119] Berstad et al.[120] |
| **Solid-state-storage** | • It is safer.<br>• Large amounts of $H_2$ can be stored in small volumes at moderate temperatures and pressures.<br>• It can store $H_2$ for a long time and relatively more conveniently.<br>• It is highly efficient. | • Regeneration is required before solid storage can be reused.<br>• It can be expensive, especially for metal hydrides.<br>• Regeneration is often slow. | Abdalla et al. [11] Rusman and Dahari. [115] Zhevago et al. [116] Tarhan and Cil, [121] |
| **Cyro-compressed** | • It has more storage density than cryogenic storage.<br>• It is a safe method of $H_2$ storage | • High cost.<br>• Lack of available infrastructure. | Bhatt and Lee. [66] Moradi and |

|  |  |  |  |
|---|---|---|---|
|  |  |  | Growth. [114] |

## 5.1 Compressed gas storage

Compressed gas storage involves reducing the gas volume (while the pressure rises) to make it containable in a storage medium. Since $H_2$ has a relatively large volume for any given mass (due to its density), it is challenging to store it by compression. Moreover, its compression is energy-intensive and costly. For instance, the energy required to compress hydrogen gas to 600 bar is 20.48 MJ/Kg, while the energy needed for methane gas to 600 bar is 1.25 MJ/Kg. This difference is significant (more than 16 times higher) [124].

In compressed $H_2$ storage systems, the storage means and the compressor involved are integral parts of the system, as they significantly affect the system's safety, cost, and reliability. This section discusses two common storage means storage vessels and geological storage. $H_2$ can be stored in aquifers, depleted natural gas and oil reservoirs, salt caverns, abandoned mines, and rock caverns in geological storage. Among these, only the salt caverns have been explored so far. A detailed description of underground $H_2$ storage methodologies is presented elsewhere [122].

In contrast, storage vessels could either be at low pressure (0.95 MPa) or high pressure (>= 35 MPa) vessels [123]. Detailed information about $H_2$ storage in vessels can be found elsewhere [123]. Moreover, pressure vessels are made from various materials, and they are usually classified as Type I–V vessels [114,122,123]. Their properties are summarized in Table 7.

**Table 7:** Properties of pressure vessel types. Adapted from Elberry et al. [122], Moradi and Growth. [114], Ozaki et al. [123].

| **Pressure Vessel Type** | **Composition**<br>**(-)** | **Density of storage vessel (kg_steel/m$^3$_steel)** | **Relative cost (-)** | **Pressure Limit (MPa)** |
|---|---|---|---|---|
| Type I | Metallic (carbon steel and low alloy steel) | 1,360 | Least expensive | 50 |
| Type II | Thick metallic hooped–wrapped composite (aluminum or steel and fibre resin) | 816 to 952 | 50% more than Type I | No documented limit |
| Type III | Carbon fibre composite and aluminum (liner) | 340 to 454 | Double of Type II | 45 |
| Type IV | Polymer like HDPE (liner) and carbon fibre or carbon-glass composite | Very light | Very costly | 100 |
| Type V | Full composite (fibre reinforced shell) | 20% lighter than Type IV | Very costly | Very limited (unfit for large-scale storage) |

## 5.2 Liquefaction/cryogenic storage

Hydrogen can also be stored in liquid form at temperatures below 20 K, a method commonly referred to as cryogenic storage. In this form, the concentration of $H_2$ doubles that of compressed gas, leading to higher storage density and less storage volume. Few experimental studies have been published in this area over two decades [120].

As a result of this low boiling point (20 K), refrigeration, insulation, and vacuum superinsulation may be used to liquefy $H_2$ and maintain this liquid state [118,119,125]. For instance, refrigeration was successfully applied in the Ingolstadt and Leuna $H_2$ liquefaction plants to bring $H_2$ to 20 K temperature [126]. $H_2$ liquefaction in the Ingolstadt plant was carried out in four stages; two catalytic converters operating at isothermal conditions with liquid $N_2$ and liquid $H_2$ bath followed by two adiabatic steps. Bracha et al. [126] estimated the exergy efficiencies of the Ingolstadt and Leuna plants to be 21.0 and 23.6%, respectively. Modelling studies of large-scale plants have yielded up to 56.8% higher exergy efficiencies, with ortho-para conversion steps ranging from 2 stages to continuous technologies [120]. A detailed comparison of modelling and existing liquefiers is presented elsewhere in the literature [120].

Although liquid $H_2$ storage is a matured technology with improved gravimetric and volumetric efficiency, it still faces several challenges, including, but not limited to, high energy demand for liquefaction, storage tank cost, heat transfer, and $H_2$ boil-off [114,125]. Between 35-40% of the energy content in the stored $H_2$ is spent on liquefaction. This amount triples the energy required to store the gas by compression [118]. As a result, $H_2$ liquefaction is capital intensive with its cost, essentially dependent on the scale of production and plant location. About 60% of the capital investment is attributable to equipment costs, 30% for infrastructure, and 10% for planning [125]. These highlighted challenges, among others, have hindered and limited the application of cryogenic technology.

## 5.3 Solid-state-storage

$H_2$ can also be stored in solid-state, a more efficient method than the first two discussed because the solid material can store relatively more significant quantities of $H_2$ in smaller volumes [121]. This can be done using nanostructured materials and hydrides, with the former having relatively lower storage efficiencies, although with great potential. The latter can be classified into complex hydrides, chemical hydrides, metal hydrides, and Magnesium-based alloys.

The potential of solid-state storage to meet the rising $H_2$ storage demand has attracted attention, bringing it to the centre of recent $H_2$ storage discussions. Though most of the hydrides, like borate hydrides of Na and Li, have high $H_2$ storage capacities, they face the problem of regeneration efficiency and cost because most metals are expensive. Nitrides are promising due to the ease with which they release $H_2$ when applied to solid-state $H_2$ storage. Chemical hydrides, which are compounds of lighter elements than metals, have high storage capacity and easily decompose to $H_2$. Magnesium-based alloys are light, cheap, readily available, and have increased storage capacity but suffer from slow reaction rates even at high temperatures. This is currently a subject of further research investigation and increasing the reaction rate [121].

Kumar et al. [127] designed a large-scale metal hydride-based $H_2$ storage system (MHHSS) and studied the effect of supply pressure, temperature, and heat transfer fluid (HTF) flow rate on the absorption and desorption rates of $H_2$. They found that as supply pressure increased, the mass of

$H_2$ absorbed and the absorption rate also increased. Chauhan et al. [128] conducted a study on the uptake of $H_2$ by graphene nanoplatelets (GNP) at temperatures of 298K, 243K, and 99K and the maximum adsorption was seen at 99K and 2 bar. This result agrees with that of Kumar et al. [127] as both demonstrate the significant impact of temperature and pressure on adsorption and desorption rates of $H_2$ gas. Another experiment conducted by Souahlia et al. [129] on metal hydrides concluded that $H_2$ storage rates varied directly with the $H_2$ supply pressure. The cooling temperature also has a marked impact on absorption, especially at low supply pressure.

### 5.4 Cyro-compressed $H_2$ gas storage

This is a method of $H_2$ storage in which the gas is compressed in its supercritical state (~233°C). At this stage, the gas cannot liquefy no matter how much it is compressed. This method produces higher storage density than liquefied storage (about 10 g/L more than the liquefied storage) and is safer [114]. Although promising, the Cyro–compressed hydrogen storage method currently lacks the infrastructure for large-scale applications. A detailed discussion on this technology is outside the scope of this review but outlined by Abdalla et al. [11] and Zhevago et al. [116].

## 6. Nanomaterials for solid-state hydrogen storage

### 6.1 Carbon nanotubes

Carbon nanotubes (CNT) are promising hydrogen storage materials due to their high adsorption capacity at room temperatures, synthesizing simplicity from renewable feedstocks [130], along with their highly microporous structure, chemical stability, and low mass density [131,132]. Carbon nanotubes, made of a graphene sheet rolled into a cylindrical tube shape, are categorized as single-walled carbon nanotube (SWCNT) and multi-walled carbon nanotubes (MWCNT). The SWCNT and MWCNT are characterized with an outer diameter range of 0.4 - 2 nm and 2 - 100 nm, respectively and 0.2-5 micron in length [133]. A conceptual diagram outlining the dimensions of SWCNTs and MWCNTs is given in Fig. 6.

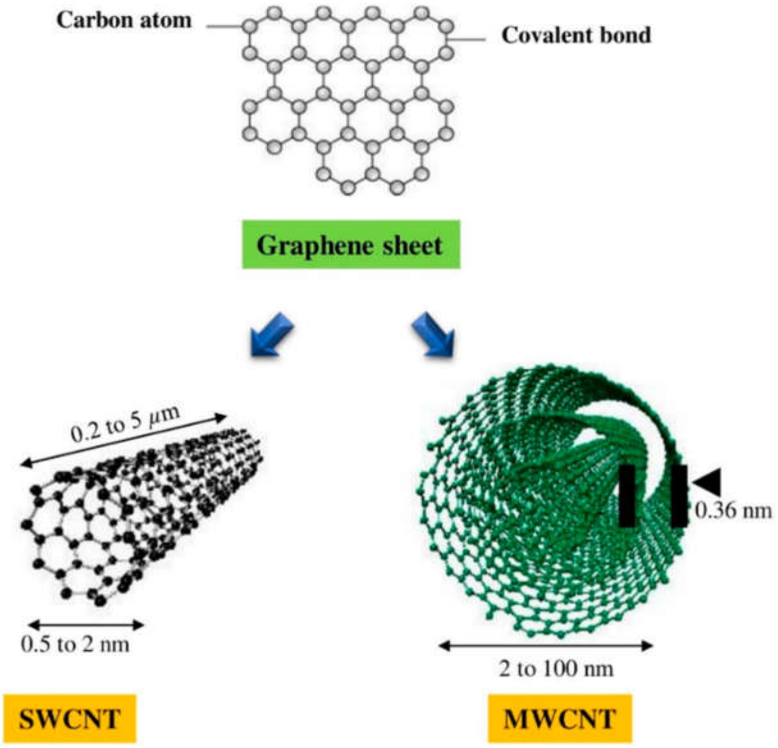

**Figure 6**. Typical structure and dimensions of SWCNTs and MWCNTs. Reprinted from Patel et al. [134] with permission from Elsevier.

The electrical, thermal, mechanical characteristics of the SWCNT and MWCNT and production technologies are recently reported in detail by Patel et al. [134]. The structure, geometry, accessible surface area purity of the CNT, and the operating temperature and pressure, are the key factors affecting the hydrogen storage capacity [135]. Experimentally measured hydrogen storage capacities of different types of CNTs are given in Table 8.

**Table 8**. Hydrogen storage capacity of the various CNTs

| | **Hydrogen Storage (wt%)** | **Loading Temperature (K)** | **Loading Pressure (MPa)** | **References** |
|---|---|---|---|---|
| CNT | 9.6 | 77 | 10 | Cheng et al. [130] |
| SWCNT | 4.5 | 77 | 6 | Panella et al. [136] |
| SWCNT | 4.5 | 298 | 0.4 | Mohan et al. [135] |
| MWCNT | 6.3 | 298 | 14.8 | Mohan et al. [135] |
| SWCNT (low purity) | 5-10 | 406 | 0.04 | Park and Keane. [137] |

| | | | | |
|---|---|---|---|---|
| SWCNT (high purity | 8.25 | 80 | 7 | Li et al. [138] |
| Aligned SWCNT | 4 | 298 | 11 | Chem et al. [139] |
| SWCNT | 11.2 | 77 | 10 | Dillon and Heben. [140] |
| Li-doped MWCNT | 20 | 200-400 | 0.1 | Dillon et al. [141] |
| K-doped MWCNT | 14 | 300 | 0.1 | Dillon et al. [141] |
| K-doped MWCNT | 1.8 | <313 | 0.1 | Huang et al. [142] |

The theoretical maximum hydrogen storage capacity of SWCNT was initially reported to be 5-10 wt% of CNT by Dillon et al. [143]. However, the possibility of reaching 11.2 wt% (Table 8) was predicted and achieved in a study conducted by Dillon and Heben [140]. The increase in the carbon storage capacity was attributed to arranging the carbon structure in a square lattice instead of a hexagonal lattice and the operation conditions 77K and 10MPa [140]. However, hydrogen storage at 77 K would not be feasible for onboard transportation on a commercial scale [132]. Therefore, most research focuses on hydrogen storage at around ambient temperature (~278).

On the other hand, MWCNTs can achieve higher hydrogen storage due to their greater surface-to-volume ratio. Their multi-layered nature allows the potential hydrogen uptake in between the multiple graphene sheets [144]. However, the overall hydrogen storage capacity of the MWCNT depends on operational conditions and the purity level, as the increased purity is directly linked to the increased number of available sites for hydrogen adsorption [145]. Ioannatos et al. [145] reported higher hydrogen storage capacities with higher purity CNTs when the operating temperature was 298 K. The CNT synthesis methods and structural modifications play an essential role. Mechanically bent CNTs are theoretically proven to have better thermodynamic properties owing to their ΔH value of the adsorption process is being in the range of 20–50 kJ/mol $H_2$, in comparison to the regular CNTs, which are likely to have thermodynamic dead end with a ΔH smaller than zero or greater than 80 kJ/mol $H_2$ [146]. Similarly, cup-stacked carbon nanotubes (CSCNT) have shown a 25% increase in hydrogen storage (has risen 1.13 w%) in comparison to regular MWCNT [131].

## 6.2 Carbon nanocomposites

Carbon-based nanocomposites are multi-constituent materials with high specific areas and low-cost processibility. Besides, they are highly attractive for solid-state hydrogen storage [147,148]. They exhibit excellent sorption kinetics due to their physicochemical attributes and facilitate low-temperature desorption due to the presence of carbon as a metal-free dehydrogenation catalyst [148–150].

Advanced concepts such as nanoconfinement, using suitably selected carbonaceous nano-scaffold/nano-porous frameworks constitute promising routes for realizing reversible solid-state hydrogen storage solutions [151,152]. Moreover, the presence of carbon can also enhance desorption rates in nanocomposites by inhibiting the formation of undesirable ternary intermediates, which can form during sorption and limit rehydrogenation (and invariably reversibility) [149,153,154].

The inherent tailorability of the constituents of these nanocomposites renders them exceptionally tuneable. Factors like pore size can play a significant role in tailoring the sorption/desorption kinetics [154,155]. It has been shown by Sepehri et al. [156] that a reduction in pore size from 16 nm to 7 nm for carbon cryogel-ammonia borane nanocomposites results in a corresponding 20% reduction in activation energy for desorption from 150 kJ/mol and up to 9% in peak dehydrogenation temperatures. These trends are in agreement with those reported by Gross et al. [151], who observed a 7% reduction in activation energy for desorption by decreasing pore size by 48% in carbon-based $LiBH_4$ nanocomposites. Unsurprisingly, an increase in micro-pore volume can yield better high-pressure and low-pressure hydrogen adsorption capacity for Nickel-activated carbon nanocomposites [157].

It has been suggested that the viability of carbon-based nanoconfinement of light metal hydrides for hydrogen storage applications depends significantly on the purity, functionality, and surface properties of the carbon employed. These factors are believed to influence the reaction pathways and thus, ultimately control desorption efficiency and reversibility. Comparing the reversibility of carbon nanocomposites with high and low oxygen-based functionality on the carbon constituent, Gao et al. [154] reported a reduction from 95% to 66% with successive rehydrogenation cycles. Interestingly, despite reporting the presence of hydroxyl and carboxyl groups on the surface of hexagonal mesoporous carbon frameworks used in their analysis, Li et al. [152] did not remark on the possible effects of these oxygen-rich functional groups on the irreversibility of the carbon-based ammonia borane nanocomposites investigated in their study. However, the authors did highlight the beneficial effects of nanoconfinement in suppressing the evolution of volatiles, which (owing to the risks of catalytic poisoning) precludes ammonia borane in hydrogen storage applications.

The importance of the appropriate selection of the carbon constituent cannot be undermined. For example, when combined with ammonia borane, carbon cryogels can suppress ammonia and reduce dehydrogenation onset temperatures, whereas activated carbon can initiate room-temperature dehydrogenation [158]. Another important consideration for using carbon nanocomposites is that some carbon species can enhance sorption kinetics by reducing the desorption temperature and participating in reversible hydrogen storage. This can be observed in $LiBH_4$-$C_{60}$ nanocomposites where hydrogenation potential can be exploited with the lithium borohydride and fullerene [150]. Table 9 summarizes some desorption characteristics of binary and ternary carbon nanocomposites in recently published works.

**Table 9:** Comparative summary of sorption and desorption parameters reported in published literature.

| **Non-carbon constituents** | **Carbon-based constituent** | **Preparation methodology** | **$^{a}$ $W_c$ (%)** | **Pore size (nm)** | **Desorption capacity (wt%)** | **$^{b}$ $T_D$ (K)** | **$^{d}$ $E_{a,D}$ (kJ/mol)** | **References** |
|---|---|---|---|---|---|---|---|---|
| Mg–Nb@* | Amorphous carbon layer | Reactive gas evaporation | – | 2** | 4.8 | 573 | 59.7 | Zhu et al. [159] |
| $Mg(BH_4)_2$–* | Carbon aerogel | Melt infiltration | 90 | 10 | – | 433 | 102 | Yan et al. [149] |
| Mg–* | Carbon aerogel | Infiltration | 77.5 | 19 | 2.15*** | 623 | 29.4 | Liu et al. [160] |
| | Carbon aerogel | | | | | | 111 | Gross et al. [151] |
| $LiBH_4$–* | Mesoporous carbon | Solution impregnation | 67 | 4 | 3.4 | 573 | – | Cahen et al. [161] |
| $LiBH_4$–$Mg(BH_4)_2$* | Activated carbon *IRH33* | Melt impregnation | 72 | <4 | 4 | 573 | – | Zhao-Karger et al. [153] |
| AB–* | Carbon cryogel | Solution impregnation | 76 | 2-50 | 9 | 358-383 | 120-150 | Feaver et al. [155], Sepehri et al. [156] |
| | Lithium-doped mesoporous carbon *Li-CMK-3* | Solution impregnation & calcination | 50 | 4.54 | 7 | 333 | 98 | Li et al. [152] |
| | Graphene | High-energy ball milling | 67 | – | 4.5 | 386 | – | Bravo Diaz et al. [158] |
| | Activated carbon | High-energy ball milling | 60 | – | 5.4 | 277 | 34 | Bravo Diaz et al. [158] |
| | Activated carbon | Solution impregnation | 60 | – | 5.4 | 285 | – | Bravo Diaz et al. [158] |

$^{a}$ $\boldsymbol{W_c}$: *Weight fraction of carbon constituent (%);* $^{b}$ $\boldsymbol{T_D}$: *Desorption temperature (K);* $^{c}$ $\boldsymbol{t_D}$: *Desorption time at* $T_D$ *(min);* $^{d}$ $\boldsymbol{E_{a,D}}$: *Activation energy for desorption.* The use of * denotes the carbon-based *constituent; ** denotes a layer thickness; *** denotes a sorption capacity.*

## 6.3 Activated carbon

Activated carbon (AC) is a physically or chemically modified form of carbon consisting of small graphite crystallites and amorphous carbon with a specific surface area of 3000 $m^2/g$. In physical activation, the starting material is carbonized at high temperatures (700-1000°C) by steam or $CO_2$. In contrast, chemical activation treats the starting materials (i.e., lignocellulosic biomass, anthracite, coal precursor etc.) with chemicals such as $H_3PO_4$, KOH, NaOH, $H_2SO_4$, and $ZnCl_2$at 500-800°C [162] [163]. It should be mentioned that $ZnCl_2$ is not a desirable activating agent due to zinc emissions in the environment.

AC is suitable for both physisorption and hydrogen chemisorption due to its large surface area and microporosity. However, choosing the right activating agent and precursor for the individual applications is vital as these are the significant factors affecting the pore size and structure [164]. The KOH activation has been reported to be a particularly suitable method of hydrogen sorption as it provides large surface areas, large pore volumes with a 1-2 nm uniform micropore size distribution in the structure [144]. The result of the recent studies is given in Table 10.

**Table 10:** Hydrogen storage capacity of various AC

| **AC Precursor** | **Hydrogen Storage (wt%)** | ***S$_{BET}$ (m$^2$/g)** | **Activating Agent** | **Loading Temperature (K)** | **Loading Pressure (MPa)** | **References** |
|---|---|---|---|---|---|---|
| Pine lignin | 1.61<br>1.93 | 1055<br>1409 | $CO_2$ | 11 | 0.1 | Czarna-Juszkiewicz et al. [165] |
| Coal from palm oil shell | 0.29 | 640 | KOH | 268 | 0.4 | Kapasiti et al. [166] |
| Coal from palm oil shell | 6.7 | 3503 | KOH | 77 | 0.4 | Zhao et al. [167] |
| Spent coffee beans | 0.6<br>0.4 | 2070<br>2070 | KOH | 298<br>77 | 12<br>4 | Akasaka et al. [168] |
| Anthracite | 3.2<br>6.0<br>5.7<br>2.7 | 1149<br>2849<br>3220<br>1308 | KOH/NaOH | 77 | 4 | Fierro et al. [169] |
| Carbon monolith | 1.28 | 973 | $CO_2$ | 293 | 60 | Series et al. [170] |
| Commercial AC | 0.67<br>5.7 | 1060<br>3306 | N/A | 303<br>77 | 10<br>3 | Xu et al. [171] |
| Anthracite | 6.6 | 3441 | KOH | 77 | 4 | Izquierdo and Celzard. [172] |
| Anthracite | 5.5 | 2451 | KOH/ Pd doped | 298 | 8 | Zhao et al. [173] |

* BET (Brunauer-Emmett-Teller) analysis to measure the specific surface area available for adsorption.

The hydrogen storage capacity is mainly dependent on the specific surface area, the bulk density, and the loading temperature. Improved hydrogen storage capacities are achieved with the experiments conducted under cryogenic conditions with moderate pressure (1-10 MPa). In contrast, an average of 3 wt.% hydrogen sorption was seen in the experiments carried out at around room temperature due to the weak interaction between the adsorbate ($H_2$) and the adsorbent (AC) at room temperature. However, the reversible hydrogen storage capacity can be enhanced by heteroatom doping as it dissociates the chemically bonded $H_2$ and subsequently allows the diffusion of hydrogen atoms into the pores [144].

Chemical activation is another essential technique that impacts the hydrogen storage capacity as it is directly linked to stimulation of micropores and correspondingly an increased adsorbent porosity. The pore structure is also dependent on the activation temperature and the KOH/precursor weight ratio. Furthermore, combined chemical and physical activation, using $CO_2$, was reported to be effective in creating more micropores which resulted in an increased specific surface area [165].

## 6.4 Complex hydrides

Complex metal hydrides (CMH) are a class of compounds with the general formula $M(XH_n)_m$, where M usually represents a metal cation, whereas X is a metal or nonmetal element, which is covalently bonded to hydrogen [174]. These compounds are hydrogen-rich and can be selectively decomposed to produce $H_2$; thus, making complex hydrides of lightweight elements efficient $H_2$ storage media. Complex hydride hydrogen storage mechanism occurs as a two-stage process involving dihydrogen dissociation into surface H atoms and the subsequent diffusion of the H atoms into the bulk phase [175]. The many possible combinations of $H_2$ with elements like nitrogen boron, oxygen, carbon, aluminum, and transition metals for CMH formation is an attribute that allows functional property modification for $H_2$ storage purposes [176].

In comparison to other $H_2$ storage methods such as liquefaction, compression, and metal-organic framework (MOF), CMHs have high $H_2$ density with the capability of de/rehydrogenation without the requirements of very high pressures and low temperatures [177]. Ley et al. [178] reported that only 0.034 $m^3$ $H_2$ stored in $\delta$-$Mg(BH_4)_2$ is required to power a family car for 500 km. This volume is significantly smaller than the equivalent 60 $m^3$ of $H_2$ required when standard fuel-cell-based storage is applied at ambient temperature and pressure. This volumetric storage efficiency is one of the factors that has led to extensive research contributions relating to the use of CMH for $H_2$ storage. However, their strong interaction with $H_2$ ($40 \leq \Delta H_{ads} \leq 100$ kJ/mol), very high desorption temperatures (> 350 °C), irreversibility issues, slow kinetics, and challenging synthesis procedures are formidable hindrances to their successful implementation [179]. For example, the thermal decomposition of $LiAlH_4$ yields $Li_3AlH_6$ and Al, which is accompanied by an exothermic release of $H_2$ gas. This initial exothermic decomposition has been shown to hinder the complete reversibility of the system [176].

Research efforts targeted at mitigating these challenges have led to the development of several thermodynamic and kinetic improvement strategies [175]. These include nanoconfinement via the application of nanoporous hosts for interface contact improvement [180], catalytic modification for enhancing $H_2$ sorption and desorption [181], and compositional alteration via anionic or cationic substitution for composites formation in the CMH [182]. We present a discussion of past contributions in light of these advancements while capturing the different classes of CMHs (including alanates, borohydrides, amide-hydride composites, as well as metalorganic hydrides).

Alanates, a class of widely explored CMHs are generally composed of a metal cation and the $[AlH_4]$-/$[AlH_6]_3^-$ anion, with storage capabilities of up to 10.4 wt.% ($LiAlH_4$), 9.3 wt.% ($Mg(AlH_4)_2$) and 9.7 wt.% ($LiMg(AlH_4)_3$), respectively [175]. $NaAlH_4$ is the most extensively studied alanate, given its relatively high gravimetric and volumetric $H_2$ densities, moderate heat of de/rehydrogenation, and low cost of raw materials [183]. The successful application of $NaAlH_4$ as $H_2$ storage material, when combined with catalysts such as nano-TiN to reduce the dissociation temperature, instigated the search for other compatible metals [184]. Transition and rare earth metals, such as Ti, Nb, Ce, Sm, Sc, have been applied via ball milling and wet doping methods to reduce further the temperature required for the commencement of dehydrogenation [178,180]. Nanoparticles such as $CeO_2$, $CeB_6$, and $CeFe_3$ have been applied to improve the hydrogenation duration of $NaAlH_4$ CMHs with timeframes as low as 20 mins observed [185]. The use of $NaAlH_4$ confined in carbon fibres has been reported to rapidly decrease the $H_2$ desorption temperature to 70 ºC [186]. Similarly, $NaAlH_4$ confined in ordered mesoporous silica achieved dehydrogenation within a temperature range of 125–150 ºC [187]. Ti and $TiO_2$ nanoparticles embedded in amorphous carbon have also shown promising potential for enhancing the $H_2$ storage capability of $NaAlH_4$, with remarkable stability obtained after 100 adsorption/desorption cycles [188]. TiN nanoparticles (nano-TiN@N-C) have also been demonstrated as reliable candidates for enhancing the thermodynamics and kinetics of $NaAlH_4$ de/rehydrogenation [189,190]. Arora et al. [191] employed DFT to explain the significant impact of experimental conditions (environmental effects) on the thermodynamic stability (the free energy of formation) of metal-doped-$NaAlH_4$. Similarly, DFT calculations implemented by Kang et al., [192] further verified the dependence between the reaction energy and the chemical environmental conditions as well as the morphological features.

Interest in metal borohydrides has been spurred by their very high $H_2$ contents and the existence of a correlation between their experimentally determined decomposition temperature and the metal's electronegativity (which strongly coordinates to the $BH_4^-$ anionic groups) [178]. One of the first studies to propose the use of metal borohydrides as an $H_2$ storage medium was that of Zuttel et al. [193], achieving a $H_2$ capacity of up to 18.5 wt.%. Recently, the nanoconfinement of $Ca(BH_4)_2$ and $Mg(BH_4)_2$ into porous hosts ($Cu_2S$) has been actively investigated; dehydrogenation at 50 °C and full rehydrogenation at 300 °C were achieved [194]. The kinetic improvement of $H_2$ storage over $M(BH_4)_m$ and $M(NH_2BH_3)_m$ has been demonstrated using catalytic dopants (including $Fe_2O_3$ and $SiO_2$) [195]. Bimetallic and trimetallic borohydrides and neutral molecule-modified metal borohydrides (e.g. $LiK(BH_4)_2$, $Li_3MgZn_5(BH_4)_{15}$, $Li_2Al(BH_4)_5{\cdot}6NH_3$), have also demonstrated $H_2$ storage capabilities as documented by Møller et al. [176]. Nanoporous $\gamma$-$Mg(BH_4)_2$ has been shown to efficiently store $H_2$ via adsorption onto the hydride's inner surface and via chemical bonding to Boron [178]. Similarly, a study by Chen et al. [196] demonstrated kinetic barrier reduction for enhancing the reversibility of $Mg(BH_4)_2$ using $MgH_2$ nanoparticles. A recent study by Wood et al. [197] showed that mechanical stresses posed by an external confining medium could affect the thermodynamics and kinetics of phase transformations that occur during the de/rehydrogenation of some CMHs; they focused on incorporating more realistic effects in their models which are usually neglected in computations based on ideal conditions.

Some unresolved challenges still plague the application of metal borohydrides for $H_2$ storage. The exact mechanism of dehydrogenation and rehydrogenation of metal borohydrides is not well understood (a possible consequence of the complex boron-hydrogen chemistry); furthermore, the avoidance of effects such as diborane release, and the segregation of amorphous boron, are still unresolved [178,193]. Moreover, alkali metal borohydrides possess higher stability (higher decomposition temperatures > 350 °C) than alkali metal alanates (with decomposition temperatures between 60 and 300 °C); on this basis, Møller et al. [176] reported that alkali metal alanates might be better suited for $H_2$ storage applications.

As with the alanates, catalytic modification can be similarly pursued with amide hydrides using transition metals, alkali metal hydrides, borohydrides, and other carbon-based materials [198].

However, these hydrides often portray very slow kinetics, which may be attributable to interface reactions, diffusion processes, and nucleation [198]. Mechanical milling is an effective method, which can be applied to mitigate this problem via grain size reduction and homogenization of the amide and hydride particles [199]. This process has been applied to $K_2[Zn(NH_2)_4]$ as documented in Cao et al. [198]. A further effect of this milling process is lowering the decomposition temperature [176].

The presented discussion demonstrates a need to develop further methods for stabilizing $H_2$ storage capacity at ambient conditions and particularly for long-term multiple usages. A primary safety concern worth mentioning here relates to alanates, which have very high reactivity with water – yielding large amounts of heat [174]. This exothermic hydrolysis reaction can initiate the hydride's thermal decomposition in the case of accidental exposure to large amounts of water. Besides storage capacity improvements, the operational safety of this $H_2$ storage technology is also worth investigating further. Moreover, a comparison of different classes of CMHs is presented in Table 11.

**Table 11:** Comparison of the different classes of CMHs.

| **Class of CMH** | **Advantages** | **Limitations** | **References** |
|---|---|---|---|
| **Alanates** | • Favourable dehydrogenation enthalpies<br>• Rapid kinetics<br>• Moderate $H_2$ capacities<br>• Relatively easy preparation with readily available components | • Insufficient reversible capacities for rehydrogenation<br>• Contact with water is a safety concern | Orimo et al. [174], He et al. [175] |
| **Borohydrides** | • High gravimetric $H_2$ capacities | • Very slow kinetics<br>• Side product formation (diborane)<br>• Irreversibility<br>• Poorly understood de/rehydrogenation mechanism | Let et al. [178], Møller et al. [176] He et al. [175], Luo et al. [180] |
| **Amide-Hydride** | • Good thermodynamic stability<br>• Moderate $H_2$ capacities | • Very slow kinetics<br>• Side product formation (mainly ammonia) | Orimo et al. [174], He et al. [175] |

## 6.5 Metal-organic frameworks

Metal-organic frameworks (MOFs), otherwise called porous coordination polymers, are a category of porous materials formed from metal ions or metal-containing nodes (secondary building units – mostly d-block transition metals) and organic linkers or multidentate ligands joined by coordinate bonds [200]. The available number of binding sites for these ligands at the metal centre often ranges from 2–12, yielding linear, cubic, octahedral, tetrahedral geometries [201]. An essential requirement in the selection of ligands for the development of porous MOFs is that the overall network be neutral. Otherwise, charged networks will cause the positioning of counter ions within the framework, which eventually reduces the porosity and $H_2$ storability of the framework material [202,203]. Unlike mesoporous oxide-based materials like zeolites, the structure and topology of the interior surface (of MOFs) on which $H_2$ is adsorbed can be easily modified for $H_2$ storage enhancement (via metal selection and ligand functionalization) [204]. MOFs' modular construction and large surface areas and pore volumes allow for this modification [205].

According to the ultimate target set by the US Department of Energy (DoE), onboard $H_2$ storage systems should be able to achieve a gravimetric capacity of 6.5 wt.% (U.S Department of Energy, 2017). Although MOFs such as (MOF-5) have already surpassed the ultimate DoE targets (in terms of gravimetric capacity) [207], sufficiently high surface area & pore volume and the formation of viable (high-energy) $H_2$-binding sites (within the framework) are essential factors for the continual development of other high-capacity MOFs, as well as their sustained cyclic performance. While the first factor influences the $H_2$ uptake rate, the second influences the $H_2$-framework interaction. Thus, the kinetics and thermodynamics of $H_2$ uptake and release must be accurately considered, for effective $H_2$ storage capacity. MOFs can also potentially address the limitations of other physisorbents (such as activated carbon and zeolites, which yield a similar $H_2$ uptake at low temperatures but have reduced $H_2$ affinity at ambient temperatures) and chemical sorbents (e.g., hydrides, which possess reasonably high $H_2$ uptakes but poor release kinetics and thermodynamics). Storage methods, which utilise chemical sorbents (like CMHs) particularly suffer from the very tight binding of $H_2$ ($\Delta H_{ads}$ in the range of 50 to 200 kJ/mol); in contrast, the $\Delta H_{ads}$ of physisorption techniques is minimal [208].

Isorecticular metal-organic frameworks (IRMOF) based on $Zn_4O$ are some of the widely studied MOFs. The earliest demonstration of the $H_2$ storage capability of MOFs was reported by Yaghi et al.[209]. Since this contribution, many MOFs have been studied with different $H_2$ storage potentials [200]. These studies have applied several routes for increasing the $H_2$ uptake, e.g. surface area and pore volume enhancement via increasing the ligand length, implementing mixed ligands, and supercritical $CO_2$ drying [210,211]. More so, the use of multifunctional groups within the same framework has also been demonstrated, with up to 84% improvement attained [212]. A summary of some key methods of improving the $H_2$ uptake capacities of MOFs is presented in Table 12.

**Table 12:** Some applied methods for improving MOF performance.

| **Method** | **Comments** | **References** |
|---|---|---|
| Sample preparation and activation via drying | Compared to traditional MOF pre-treatment methods (soaking samples in low boiling point solvents for porosity enhancement), freeze-drying and supercritical drying have been shown to improve pore performance significantly. | Ma et al. [213], Cooper and Rosseinsky. [214], Xiang et al. [215] |
| Unsaturated metal sites modification | These sites show significant $H_2$ binding potential and are usually the first loading sites for $H_2$ molecules. This depends on the cationic radius of the exposed metal site. Thermal-based activation has been applied to access the increased gas-adsorption potential of a MOF material. | Zhou et al. [216], Bagheri et al. [217] |
| Catenation/ Interpenetration | While this method increases the interaction between the framework and H atoms, it may also result in reduced pore volume, consequently reducing $H_2$ storage. The effect of this method is also somewhat pressure-dependent. | Sule et al. [204], Zelenák and Saldan [202] |
| Functionalization of ligand structure | Covalent, coordinate, and covalent-coordinate modification are the primary enhancement routes. Aromatic substituents have shown promising potential for functionalizing ligand structures (due to additionally provided binding sites); thus, yielding improved $H_2$ uptake compared to the pristine MOFs. | Rowsell et al. [218] |
| Chemical doping | This is a post-synthetic modification method using metals like cationic or atomic Lithium. As high as 7.5 times the storage capacity of the undoped IRMOF-14 has been reported using lithium. Doping with metal nanoparticles such as palladium nanoparticles is also a promising approach to achieving $H_2$ storage at ambient conditions. | Mavrandonakis et al. [219], Cheng et al. [220] |
| Crystal size and morphology control | A strategy that enhances MOFs' poor volumetric packing/storage density has been presented in the literature. Packing density enhancement is achieved using the benchmark sorbent, MOF-5. | Suresh et al. [221] |
| Rapid evaluation of the surface area and pore volume | An empirical expression correlating the pore volume (*V*) or surface area (*S*) to the $H_2$ uptake of selected MOFs allows the prediction of the sorption capacity of a new MOF using it *V* and *S* alone. | Kolotilov and Pavlishchuk. [222] |

High storage capacities and rapid release kinetics have maintained MOFs at the forefront of established $H_2$ storage methodologies in light of the US Department of Energy (DoE) ultimate $H_2$ storage targets. Increasing MOF-$H_2$ interactions at ambient temperatures and their volumetric packing efficiency are areas that will benefit from further investigations; thus, aiding the technological translation of this $H_2$ storage method. Fig.7 compares the performance of different $H_2$ storage materials with the DoE ultimate targets.

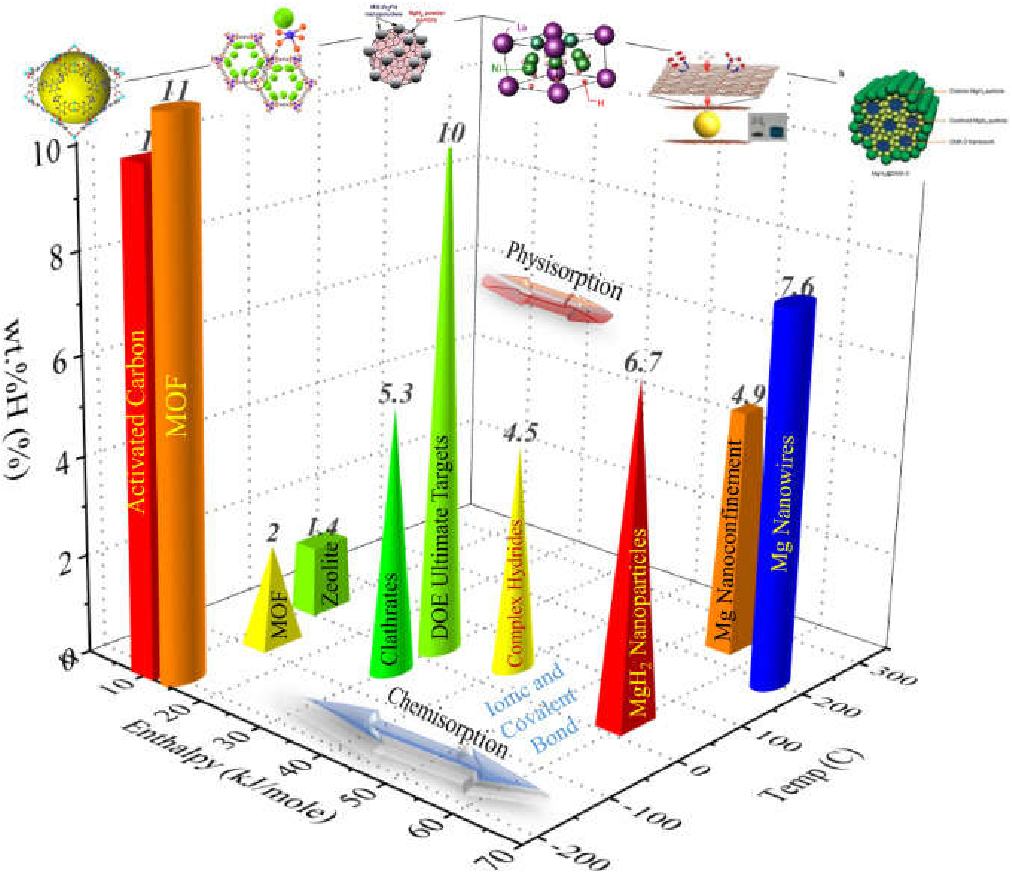

Figure 7: Comparison of different $H_2$ storage materials. Reprinted from Gupta et al. [179] with permission from Elsevier.

## 6.6 Hydrogen storage in clathrates

Clathrate hydrates or hydrogen hydrates are compounds that incorporate guest molecules inside a host framework (polyhedral cages) comprising of $H_2$-bonded water molecules – on mixing water and $H_2$ gas at low temperatures, and high pressures, the guest molecules ($H_2$) are entrapped into the polyhedral cages of the host framework to form the hydrate [223]. Hydrogen bonding, van der Waals (dispersion) forces, and intermolecular interactions govern this process and are linked to the structure's stability [224]. Without the encasement and corresponding support of these gas molecules, the structure of the hydrogen hydrates collapses into the water. Table 13 shows the structural properties of typical hydrate structures.

**Table 13:** Structure of commonly formed hydrogen hydrates Chattaraj et al. [225].

| **Type** | **Number of water molecules** | **Unit cell structure** |
|---|---|---|
| sI | 46 | Two pentagonal dodecahedron ($\mathbf{5}^{12}$) and six hexagonal truncated trapezohedron ($\mathbf{5}^{12}\mathbf{6}^{2}$) cages. |
| sII | 136 | Sixteen $\mathbf{5}^{12}$ and eight $\mathbf{5}^{\mathbf{12}}\mathbf{6}^{4}$ cages. |
| sH | 36 | Three $\mathbf{5}^{12}$, two $\mathbf{4}^{\mathbf{3}}\mathbf{5}^{6}\mathbf{6}^{3}$, and one $\mathbf{5}^{12}\mathbf{6}^{8}$ cages. |

A pioneering study by Mao et al. [226] demonstrated that pristine $H_2$ hydrates could store as high as 5 wt.% of $H_2$ at a pressure of 200 MPa and 243 K. This elevated pressure is a severe concern that limits its usage in mobile applications. One notable approach to mitigate this high-pressure requirement for $H_2$ hydrate formation is to develop binary hydrates which contain a helper molecule (gas or liquid) and $H_2$ as the second molecule. Further developments by Florusse et al. [227] involved the application of a water-soluble compound (THF) as an additive to significantly reduce the formation pressure to 5 MPa at 279.6 K; however, this caused a substantial drop in the $H_2$ storage capacity (1 wt.%).

Through the use of promoters such as THF, TBAB, and TBPB, Du et al. [228,229] formulated $H_2$ hydrate at ambient pressure conditions. The effect of a simultaneous change in temperature and pressure has been shown to be favourable on the formation rate of $H_2$ hydrates (21% increase) while using a THF promoter [230]. Liu et al. [231] performed *ab initio* molecular dynamics simulations to investigate the impact of THF on $H_2$ storage capacity in clathrates and obtained capacities between 1.6 and 3.8 wt.% depending on THF concentration. Their computations also illustrated that a single $H_2$ molecule occupies the small cages of the hydrate, whereas the large cages are likely to contain one THF molecule together with one $H_2$ molecule. Ghaani et al. [232] utilized non-equilibrium molecular dynamics (NEMD) simulations to analyze $H_2$ release and uptake from propane planar clathrate surfaces at 180-273 K. The obtained experimental $H_2$ storage capacity (using a fixed bed reactor) was 1.04 wt.% in comparison to the theoretically obtained 1.13 wt.% of the propane hydrate. A novel dual-function (thermodynamic and kinetic) promoter, 1,3-dioxolane (DIOX), was proposed by Zhang et al. [233]  for $H_2$-bearing sII hydrate formation. Within 2 h, a $H_2$ uptake of up to 26.51 v/v (gas/hydrate) was attained, corresponding to a 30.2% increase over the maximum $H_2$ uptake obtained using the conventional THF promoter. Besides the above-mentioned promoters, other suggested promoters explored in the literature include tertiary alcohols [234],  argon [235] , nitrogen [236], alkyl amines [237], methane [238], and $SF_6$ [239]. A summary of important promoter molecules used in the past 20 years and their $H_2$ storage properties is presented in Gupta et al. [179].

Despite the recent developments in enhancing the thermodynamics of $H_2$ hydrate storage performance, formation and stabilization at moderate conditions, improving hydrate formation kinetics is still a formidable challenge. The kinetics of hydrate formation in supercooled water-hydrogen solution (without promoters) has been studied by del Rosso et al. [240] at 2000 bar and 263 K. It was postulated that the diffusion rate of $H_2$ limits the rate of hydrate formation through the liquid phase. Immediately the transformation to solid is complete (after 18 h), the reaction rate rapidly increases.  The application of surfactants, nanoconfinements, and guest molecule replacement (mainly via computational methodologies) are emerging research trends targeted at resolving this problem of slow kinetics [241–243]. Recent developments by Di Profio et al. [244], which apply a reverse micelles formation method, have shown significantly reduced time of $H_2$ hydrate formation (20 – 30 mins) using promoters like THF, THT, CP, and THT.

An important advantage of $H_2$ hydrate systems is the rapid and straightforward release of $H_2$. Thus, no chemical reactions are needed for $H_2$ release since the binding energy is minimal [224](Struzhkin et al., 2007). This eliminates the possibility of high dissociation heat requirements as with metal hydrides. Stirring and the use of memory water (previously used water for hydrate formation) have been investigated for further improving the release rate [230,241,242]. This memory effect of water (during freezing and refreezing cycles) can be attributed to the occurrence of microscopic hydrate residues in the water phase after low-temperature melting. These residues subsequently act as nuclei for recrystallization during the hydrate formation phase, thus accelerating the formation process [245]. One of the most recent studies [246], which experimentally illustrated this memory effect, further confirmed this earlier proposed mechanism.

## 7. Perspectives and future directions

Nanomaterials have shown great promise in biological hydrogen production; however, the mechanism of nanomaterial-influenced hydrogen production via biological routes is not well understood. Moreover, the nanomaterial integrated approach for biological hydrogen production is a study area that has not been explored. For instance, the combination of photo fermentation and dark fermentation assisted with nanomaterials is an area that has not been explored. Integration of different biological routes could provide new insights into the development of optimal and cost-effective hydrogen production processes.

As far as nanoelectrocatalytic and nanophotocatalytic $H_2$ production is concerned, the development of 2D nanomaterials with hybrid structures and multifunctional properties may provide new opportunities to enhance their $H_2$ production potential via water splitting. Their large-scale production in controlled environments is also worth investigating; however, this is dependent on the novel research endeavours which provide insights into the complex catalytic mechanisms rather than their catalytic performance for $H_2$ production alone.

Further research on the application of physisorbents materials (particularly activated carbon and MOFs) for $H_2$ storage may focus on designing new functional materials with higher surface areas and pore volumes, increased hydrostability, and sufficient interaction energy the retainment of $H_2$ at ambient temperatures. Furthermore, the application of carbon nanotubes for $H_2$ storage is significantly affected by the purity and uncertainties governing their preparation. Further research developments in this area may target robust synthesizing procedures that yield increased purity and thus better $H_2$ storage capability. There is a need to study the effect of oxygen-rich carbon groups on the reversibility of carbon-based nanocomposites; this is particularly important for ammonia-borane variants. In addition, the identification of carbon-based nanomaterials that afford the enhancement in adsorption kinetics and the ability to participate in the reversibility of hydrogen storage is vital.

The hybrid application of earlier-discussed improvement strategies for CMHs (e.g. nanoconfinement and catalytic doping) has strong potential to enhance their performance further and requires further analysis. As earlier pointed out, the mechanisms of dehydrogenation and rehydrogenation of some CMHs are not well understood (e.g., the mechanism of $H_2$ dissociation and diffusion into and out of the bulk phase); this also increases the difficulty of distinguishing the main mechanism of performance improvement when enhancement strategies are applied. These strategies are also often associated with a high synthesis cost; more research endeavours are required for simplification and cost reduction. The sensitivity of CMHs to air makes their characterization difficult for $H_2$ storage analyses; thus, novel technologies are required for efficient characterization. Accidental exposure of CMHs (particularly alanates) to large amounts of water may instigate their thermal decomposition. Safety analyses of their large-scale application is also worth investigating.

The presented discussion has summarized some of the challenges associated with $H_2$ hydrate systems, including (extreme operating conditions in the absence of a promoter, slow formation kinetics, low storage capacity, prolonged cyclic storage performance uncertainties, mass transfer constraints). However, the most significant of these challenges, limiting the application of this technology for onboard storage, appears to be slow formation kinetics. Further developments are particularly needed in this direction. In addition, $H_2$ hydrate formation appears to be mainly studied using computational techniques; to enhance their accuracy via robust parameterization, more experiments on the mechanism of $H_2$ hydrate crystallization are needed. The interaction of additives has thus far been studied thermodynamically, further studies on the influence of molecule migration may further improve the current understanding of their kinetics of formation.

Computational-based research on $H_2$ storage considering practical and rigorous conditions, and accounting for practical uncertainties, need to be developed. Furthermore, a thorough economic comparison of $H_2$ storage methods is still lacking in the literature. In addition, more studies are required on the effect of industrial scaleup (particularly in terms of heat transfer) on larger samples of these materials compared to the smaller samples usually applied in laboratory experiments.

The indirect storage of $H_2$ via its conversion to light hydrogen-containing chemicals such as formic acid, methanol, methane and ammonia is also an area that requires future studies. These chemicals are easy to store and transport and provide a carbon-free chemical energy carrier solution for the transportation sector [247]. Ammonia storage, either in the liquid or gaseous form, is a mature technology and has fewer challenges than hydrogen storage [248]. Furthermore, it is easier to transport if ammonia is stored in the liquid form [247]. However, more studies are required in this field, especially in process economics and life cycle assessment, to evaluate the economic feasibility and environmental impacts of indirect hydrogen storage routes [249].

# 8. Conclusions

Nanomaterials are gaining more importance in addressing hydrogen production and storage challenges. They can be applied in almost all technological breakthroughs, including catalysis, metal-organic framework, complex hydrides, etc. This study outlines nanosized materials' specific application to improve hydrogen production and storage. Specifically, nanomaterials are very important in enhancing hydrogen yields of biological and thermochemical conversion processes.

Nanomaterials can be applied at different stages of biohydrogen production, including biomass pre-treatment, improved sugar and enzymes production, and enzymatic hydrolysis. In contrast, they can be used as catalysts and promoters during thermochemical processes. Nanomaterials could also be impregnated directly to lignocellulosic biomass before thermochemical processes. Ni and Fe are the most promising nanomaterials for $H_2$ production via thermochemical or biological processes.

Several nanosized materials can be used for solid-state $H_2$ storage in the form of CNTs, nanocomposites, AC, and MOF. All these materials have several advantages and limitations. Although most of the hydrides, like borate hydrides of Na and Li, have high $H_2$ storage capacities, they face the problem of regeneration efficiency and cost because most metals are expensive.

# References

[1] Tian MW, Yuen HC, Yan SR, Huang WL. The multiple selections of fostering applications of hydrogen energy by integrating economic and industrial evaluation of different regions. Int J Hydrogen Energy 2019;44:29390–8. https://doi.org/10.1016/j.ijhydene.2019.07.089.

[2] Nanda S, Li K, Abatzoglou N, Dalai AK, Kozinski JA. Advancements and confinements in hydrogen production technologies. Bioenergy Syst Futur Prospect Biofuels Biohydrogen 2017:373–418. https://doi.org/10.1016/B978-0-08-101031-0.00011-9.

[3] Hydrogen Properties | Connecticut Hydrogen-Fuel Cell Coalition n.d. http://chfcc.org/hydrogen-fuel-cells/about-hydrogen/hydrogen-properties/ (accessed December 17, 2021).

[4] AFDC. Alternative Fuels Data Center: Hydrogen Benefits and Considerations. US_Department_of_Energy 2017. https://afdc.energy.gov/fuels/hydrogen_benefits.html%0Ahttps://afdc.energy.gov/fuels/hydrogen_benefits.html%0Ahttps://www.afdc.energy.gov/fuels/ethanol_benefits.html%0Ahttps://www.afdc.energy.gov/fuels/hydrogen_benefits.html%0Ahttps://afdc.energy.gov/fuel (accessed December 17, 2021).

[5] Okolie JA, Patra BR, Mukherjee A, Nanda S, Dalai AK, Kozinski JA. Futuristic applications of hydrogen in energy, biorefining, aerospace, pharmaceuticals and metallurgy. Int J Hydrogen Energy 2021;46:8885–905. https://doi.org/10.1016/j.ijhydene.2021.01.014.

[6] Acar C, Dincer I. Comparative assessment of hydrogen production methods from renewable and non-renewable sources. Int J Hydrogen Energy 2014;39:1–12. https://doi.org/10.1016/j.ijhydene.2013.10.060.

[7] Boateng E, Chen A. Recent advances in nanomaterial-based solid-state hydrogen storage. Mater Today Adv 2020;6:100022. https://doi.org/10.1016/j.mtadv.2019.100022.

[8] Liu W, Sun L, Li Z, Fujii M, Geng Y, Dong L, et al. Trends and future challenges in hydrogen production and storage research. Environ Sci Pollut Res 2020;27:31092–104. https://doi.org/10.1007/s11356-020-09470-0.

[9] Reddy NL, Rao VN, Vijayakumar M, Santhosh R, Anandan S, Karthik M, et al. A review on frontiers in plasmonic nano-photocatalysts for hydrogen production. Int J Hydrogen Energy 2019;44:10453–72. https://doi.org/10.1016/j.ijhydene.2019.02.120.

[10] Mao SS, Shen S, Guo L. Nanomaterials for renewable hydrogen production, storage and utilization. Prog Nat Sci Mater Int 2012;22:522–34. https://doi.org/10.1016/j.pnsc.2012.12.003.

[11] Abdalla AM, Hossain S, Nisfindy OB, Azad AT, Dawood M, Azad AK. Hydrogen production, storage, transportation and key challenges with applications: A review. Energy Convers Manag 2018;165:602–27. https://doi.org/10.1016/J.ENCONMAN.2018.03.088.

[12] World Economic Forum. Grey, blue, green – the many colours of hydrogen explained | World Economic Forum. 2021 7AD. https://www.weforum.org/agenda/2021/07/clean-energy-green-hydrogen/ (accessed December 15, 2021).

[13] Hydrogen: grey, blue, and BC green - Resource Works n.d.

https://www.resourceworks.com/hydrogen-grey-blue (accessed December 15, 2021).

[14] Nikolaidis P, Poullikkas A. A comparative overview of hydrogen production processes. Renew Sustain Energy Rev 2017;67:597–611. https://doi.org/10.1016/j.rser.2016.09.044.

[15] Gunes B. A critical review on biofilm-based reactor systems for enhanced syngas fermentation processes. Renew Sustain Energy Rev 2021;143:110950. https://doi.org/10.1016/j.rser.2021.110950.

[16] Wang Q, Zhao Q, Wu RS, Tao XM, Zhang C. Review on copper- and palladium-based catalysts for methanol steam reforming to produce hydrogen. Xiandai Huagong/Modern Chem Ind 2019;39:50–3. https://doi.org/10.16606/j.cnki.issn0253-4320.2019.06.010.

[17] Iulianelli A, Liguori S, Wilcox J, Basile A. Advances on methane steam reforming to produce hydrogen through membrane reactors technology: A review. Catal Rev - Sci Eng 2016;58:1–35. https://doi.org/10.1080/01614940.2015.1099882.

[18] Levin DB, Zhu H, Beland M, Cicek N, Holbein BE. Potential for hydrogen and methane production from biomass residues in Canada. Bioresour Technol 2007;98:654–60. https://doi.org/10.1016/j.biortech.2006.02.027.

[19] Kim Y, Kim M, Jeong H, Kim Y, Choi SH, Ham HC, et al. High purity hydrogen production via aqueous phase reforming of xylose over small Pt nanoparticles on a γ-Al2O3 support. Int J Hydrogen Energy 2020;45:13848–61. https://doi.org/10.1016/j.ijhydene.2020.03.014.

[20] El Doukkali M, Iriondo A, Arias PL, Requies J, Gandarías I, Jalowiecki-Duhamel L, et al. A comparison of sol-gel and impregnated Pt or/and Ni based γ-alumina catalysts for bioglycerol aqueous phase reforming. Appl Catal B Environ 2012;125:516–29. https://doi.org/10.1016/j.apcatb.2012.06.024.

[21] Zoppi G, Pipitone G, Gruber H, Weber G, Reichhold A, Pirone R, et al. Aqueous phase reforming of pilot-scale Fischer-Tropsch water effluent for sustainable hydrogen production. Catal Today 2021;367:239–47. https://doi.org/10.1016/j.cattod.2020.04.024.

[22] Freni S, Calogero G, Cavallaro S. Hydrogen production from methane through catalytic partial oxidation reactions. J Power Sources 2000;87:28–38. https://doi.org/10.1016/S0378-7753(99)00357-2.

[23] Okolie JA, Nanda S, Dalai AK, Berruti F, Kozinski JA. A review on subcritical and supercritical water gasification of biogenic, polymeric and petroleum wastes to hydrogen-rich synthesis gas. Renew Sustain Energy Rev 2020;119:109546. https://doi.org/10.1016/j.rser.2019.109546.

[24] Demirbaş A. Biomass resource facilities and biomass conversion processing for fuels and chemicals. Energy Convers Manag 2001;42:1357–78. https://doi.org/10.1016/S0196-8904(00)00137-0.

[25] Demirbaş A. Yields of hydrogen-rich gaseous products via pyrolysis from selected biomass samples. Fuel 2001;80:1885–91. https://doi.org/10.1016/S0016-2361(01)00070-9.

[26] Duman G, Uddin MA, Yanik J. Hydrogen production from algal biomass via steam gasification. Bioresour Technol 2014;166:24–30. https://doi.org/10.1016/j.biortech.2014.04.096.

[27] Iribarren D, Susmozas A, Petrakopoulou F, Dufour J. Environmental and exergetic evaluation of hydrogen production via lignocellulosic biomass gasification. J Clean Prod 2014;69:165–75. https://doi.org/10.1016/j.jclepro.2014.01.068.

[28] Wang Z, He T, Qin J, Wu J, Li J, Zi Z, et al. Gasification of biomass with oxygen-enriched air in a pilot scale two-stage gasifier. Fuel 2015;150:386–93. https://doi.org/10.1016/j.fuel.2015.02.056.

[29] Fremaux S, Beheshti SM, Ghassemi H, Shahsavan-Markadeh R. An experimental study on hydrogen-rich gas production via steam gasification of biomass in a research-scale fluidized bed. Energy Convers Manag 2015;91:427–32. https://doi.org/10.1016/j.enconman.2014.12.048.

[30] Okolie JA, Rana R, Nanda S, Dalai AK, Kozinski JA. Supercritical water gasification of biomass: A state-of-the-art review of process parameters, reaction mechanisms and catalysis. Sustain Energy Fuels 2019;3:578–98. https://doi.org/10.1039/c8se00565f.

[31] Ahmad AA, Zawawi NA, Kasim FH, Inayat A, Khasri A. Assessing the gasification performance of biomass: A review on biomass gasification process conditions, optimization and economic evaluation. Renew Sustain Energy Rev 2016;53:1333–47. https://doi.org/10.1016/j.rser.2015.09.030.

[32] Kruse A. Hydrothermal biomass gasification. J Supercrit Fluids 2009;47:391–9. https://doi.org/10.1016/j.supflu.2008.10.009.

[33] Adar E, Ince M, Karatop B, Bilgili MS. The risk analysis by failure mode and effect analysis (FMEA) and fuzzy-FMEA of supercritical water gasification system used in the sewage sludge treatment. J Environ Chem Eng 2017;5:1261–8. https://doi.org/10.1016/j.jece.2017.02.006.

[34] Rodriguez Correa C, Kruse A. Supercritical water gasification of biomass for hydrogen production – Review. J Supercrit Fluids 2018;133:573–90. https://doi.org/10.1016/j.supflu.2017.09.019.

[35] Das D, Veziroğlu TN. Hydrogen production by biological processes: A survey of literature. Int J Hydrogen Energy 2001;26:13–28. https://doi.org/10.1016/S0360-3199(00)00058-6.

[36] Kapdan IK, Kargi F. Bio-hydrogen production from waste materials. Enzyme Microb Technol 2006;38:569–82. https://doi.org/10.1016/j.enzmictec.2005.09.015.

[37] Ni M, Leung DYC, Leung MKH, Sumathy K. An overview of hydrogen production from biomass. Fuel Process Technol 2006;87:461–72. https://doi.org/10.1016/j.fuproc.2005.11.003.

[38] Holladay JD, Hu J, King DL, Wang Y. An overview of hydrogen production technologies. Catal Today 2009;139:244–60. https://doi.org/10.1016/j.cattod.2008.08.039.

[39] Das D, Veziroglu TN. Advances in biological hydrogen production processes. Int J Hydrogen Energy 2008;33:6046–57. https://doi.org/10.1016/j.ijhydene.2008.07.098.

[40] Herbaut M, Siaj M, Claverie JP. Nanomaterials-Based Water Splitting: How Far Are We from a Sustainable Solution? ACS Appl Nano Mater 2021;4:907–10. https://doi.org/10.1021/acsanm.1c00246.

[41] Safari F, Dincer I. A review and comparative evaluation of thermochemical water splitting cycles for hydrogen production. Energy Convers Manag 2020;205:112182.

https://doi.org/10.1016/J.ENCONMAN.2019.112182.

[42] MarcelloDe Falco LMG laquaniello. Membrane reactors for hydrogen production processes. London, England: Springer; 2011. https://doi.org/10.1007/978-0-85729-151-6 Springer.

[43] McKendry P. Energy production from biomass (part 1): Overview of biomass. Bioresour Technol 2002;83:37–46. https://doi.org/10.1016/S0960-8524(01)00118-3.

[44] Levene JI, Mann MK, Margolis RM, Milbrandt A. An analysis of hydrogen production from renewable electricity sources. Sol Energy 2007;81:773–80. https://doi.org/10.1016/j.solener.2006.10.005.

[45] Bak T, Nowotny J, Rekas M, Sorrell CC. Photo-electrochemical properties of the TiO2-Pt system in aqueous solutions. Int J Hydrogen Energy 2002;27:19–26. https://doi.org/10.1016/S0360-3199(01)00090-8.

[46] Cao LM, Lu D, Zhong DC, Lu TB. Prussian blue analogues and their derived nanomaterials for electrocatalytic water splitting. Coord Chem Rev 2020;407:213156. https://doi.org/10.1016/j.ccr.2019.213156.

[47] energy.org. Hydrogen Production: Photoelectrochemical Water Splitting | Department of Energy 2020. https://www.energy.gov/eere/fuelcells/hydrogen-production-photoelectrochemical-water-splitting (accessed August 11, 2021).

[48] Song W, Li M, Wang C, Lu X. Electronic modulation and interface engineering of electrospun nanomaterials-based electrocatalysts toward water splitting. Carbon Energy 2021;3:101–28. https://doi.org/10.1002/cey2.85.

[49] Narwade SS, Mali SM, Digraskar R V., Sapner VS, Sathe BR. Ni/NiO@rGO as an efficient bifunctional electrocatalyst for enhanced overall water splitting reactions. Int J Hydrogen Energy 2019;44:27001–9. https://doi.org/10.1016/j.ijhydene.2019.08.147.

[50] Paul SC, Dey SC, Molla MAI, Islam MS, Debnath S, Miah MY, et al. Nanomaterials as electrocatalyst for hydrogen and oxygen evolution reaction: Exploitation of challenges and current progressions. Polyhedron 2021;193:114871. https://doi.org/10.1016/j.poly.2020.114871.

[51] Kumar S, Srivastava R, Chattopadhyay J. MxOy/M/graphene coated multi-shelled nano-sphere as Bi-functional electrocatalysts for hydrogen and oxygen evolution. Int J Hydrogen Energy 2021;46:341–56. https://doi.org/10.1016/j.ijhydene.2020.09.139.

[52] Wang B, Zhou Y, Hou Q, Han Y, Huo W, Luo T, et al. One stable electrocatalyst for two evolution reactions by one-pot combustion synthesis. Int J Hydrogen Energy 2020;45:22691–9. https://doi.org/10.1016/j.ijhydene.2020.06.077.

[53] Wan S, Hu J, Li GD, Yang L, Liu Y, Gao R, et al. Nano-netlike carbon fibers decorated with highly dispersed CoSe2nanoparticles as efficient hydrogen evolution electrocatalysts. J Alloys Compd 2017;702:611–8. https://doi.org/10.1016/j.jallcom.2017.01.207.

[54] Han HS, Yi F, Choi S, Kim J, Kwon J, Park K, et al. Self-supported vanadium-incorporated cobalt phosphide as a highly efficient bifunctional electrocatalyst for water splitting. J Alloys Compd 2020;846:156350. https://doi.org/10.1016/j.jallcom.2020.156350.

[55] Jadhav RG, Singh D, Krivoshapkin P V., Das AK. Electrodeposited Organic-Inorganic Nanohybrid as Robust Bifunctional Electrocatalyst for Water Splitting. Inorg Chem 2020;59:7469–78. https://doi.org/10.1021/acs.inorgchem.0c00227.

[56] Yan Q, Chen X, Wei T, Wang G, Zhu M, Zhuo Y, et al. Hierarchical Edge-Rich Nickel Phosphide Nanosheet Arrays as Efficient Electrocatalysts toward Hydrogen Evolution in Both Alkaline and Acidic Conditions. ACS Sustain Chem Eng 2019;7:7804–11. https://doi.org/10.1021/acssuschemeng.8b06861.

[57] Dai W, Ren K, Zhu Y an, Pan Y, Yu J, Lu T. Flower-like CoNi2S4/Ni3S2 nanosheet clusters on nickel foam as bifunctional electrocatalyst for overall water splitting. J Alloys Compd 2020;844:156252. https://doi.org/10.1016/j.jallcom.2020.156252.

[58] Kumar A, Bhattacharyya S. Porous NiFe-Oxide Nanocubes as Bifunctional Electrocatalysts for Efficient Water-Splitting. ACS Appl Mater Interfaces 2017;9:41906–15. https://doi.org/10.1021/acsami.7b14096.

[59] Zeng L, Sun K, Wang X, Liu Y, Pan Y, Liu Z, et al. Three-dimensional-networked Ni2P/Ni3S2 heteronanoflake arrays for highly enhanced electrochemical overall-water-splitting activity. Nano Energy 2018;51:26–36. https://doi.org/10.1016/j.nanoen.2018.06.048.

[60] Mugheri AQ, Daudpoto MR, Mugheri AA, Kalhoro DM. Recent progress in doping-induced structural and electronic modification in Cu–SnCo interconnected network enhanced efficient performance evidence for the hydrogen evolution reaction: current state and prospects. J Porous Mater 2021;1:1–10. https://doi.org/10.1007/s10934-021-01084-2.

[61] Wang C, Zhang P, Lei J, Dong W, Wang J. Integrated 3D MoSe2@Ni0.85Se Nanowire Network with Synergistic Cooperation as Highly Efficient Electrocatalysts for Hydrogen Evolution Reaction in Alkaline Medium. Electrochim Acta 2017;246:712–9. https://doi.org/10.1016/j.electacta.2017.06.028.

[62] Wang L, Fernández-Terán R, Zhang L, Fernandes DLA, Tian L, Chen H, et al. Organic Polymer Dots as Photocatalysts for Visible Light-Driven Hydrogen Generation. Angew Chemie 2016;128:12494–8. https://doi.org/10.1002/ange.201607018.

[63] Qian W, Xu S, Zhang X, Li C, Yang W, Bowen CR, et al. Differences and Similarities of Photocatalysis and Electrocatalysis in Two-Dimensional Nanomaterials: Strategies, Traps, Applications and Challenges. Nano-Micro Lett 2021;13:1–38. https://doi.org/10.1007/s40820-021-00681-9.

[64] Clarizia L, Russo D, Di Somma I, Andreozzi R, Marotta R. Hydrogen generation through solar photocatalytic processes: A review of the configuration and the properties of effective metal-based semiconductor nanomaterials. Energies 2017;10. https://doi.org/10.3390/en10101624.

[65] Puga A V. Photocatalytic production of hydrogen from biomass-derived feedstocks. Coord Chem Rev 2016;315:1–66. https://doi.org/10.1016/j.ccr.2015.12.009.

[66] Bhatt MD, Lee JS. Nanomaterials for photocatalytic hydrogen production: From theoretical perspectives. RSC Adv 2017;7:34875–85. https://doi.org/10.1039/c7ra03435k.

[67] Kumar R, Suyamburajan VA, Khan A, Asiri AM, Dzudzevic-Cancar H. Nanophotocatalysts for

hydrogen production applications. Nanomater Hydrog Storage Appl 2021:219–29. https://doi.org/10.1016/b978-0-12-819476-8.00018-9.

[68] Mahzoon S, Nowee SM, Haghighi M. Synergetic combination of 1D-2D g-C3N4 heterojunction nanophotocatalyst for hydrogen production via water splitting under visible light irradiation. Renew Energy 2018;127:433–43. https://doi.org/10.1016/j.renene.2018.04.076.

[69] Yu M, Zhang W, Guo Z, Wu Y, Zhu W. Engineering Nanoparticulate Organic Photocatalysts via a Scalable Flash Nanoprecipitation Process for Efficient Hydrogen Production. Angew Chemie - Int Ed 2021;60:15590–7. https://doi.org/10.1002/anie.202104233.

[70] Ganguly P, Harb M, Cao Z, Cavallo L, Breen A, Dervin S, et al. 2D Nanomaterials for Photocatalytic Hydrogen Production. ACS Energy Lett 2019;4:1687–709. https://doi.org/10.1021/acsenergylett.9b00940.

[71] Zada A, Khan M, Qureshi MN, Liu SY, Wang R. Accelerating Photocatalytic Hydrogen Production and Pollutant Degradation by Functionalizing g-C3N4 With SnO2. Front Chem 2020;7:941. https://doi.org/10.3389/fchem.2019.00941.

[72] Balasubramanian S, Wang P, Schaller RD, Rajh T, Rozhkova EA. High-performance bioassisted nanophotocatalyst for hydrogen production. Nano Lett 2013;13:3365–71. https://doi.org/10.1021/nl4016655.

[73] Li X, Hou Y, Zhao Q, Teng W, Hu X, Chen G. Capability of novel ZnFe2O4 nanotube arrays for visible-light induced degradation of 4-chlorophenol. Chemosphere 2011;82:581–6. https://doi.org/10.1016/j.chemosphere.2010.09.068.

[74] Pachfule P, Acharjya A, Roeser J, Langenhahn T, Schwarze M, Schomäcker R, et al. Diacetylene Functionalized Covalent Organic Framework (COF) for Photocatalytic Hydrogen Generation. J Am Chem Soc 2018;140:1423–7. https://doi.org/10.1021/jacs.7b11255.

[75] Kumar P, Boukherroub R, Shankar K. Sunlight-driven water-splitting using two-dimensional carbon based semiconductors. J Mater Chem A 2018;6:12876–931. https://doi.org/10.1039/c8ta02061b.

[76] Dai C, Pan Y, Liu B. Conjugated Polymer Nanomaterials for Solar Water Splitting. Adv Energy Mater 2020;10:2002474. https://doi.org/10.1002/aenm.202002474.

[77] Zhu T, Wu H Bin, Wang Y, Xu R, Lou XW. Formation of 1D hierarchical structures composed of Ni3S 2 nanosheets on CNTs backbone for supercapacitors and photocatalytic H2 production. Adv Energy Mater 2012;2:1497–502. https://doi.org/10.1002/aenm.201200269.

[78] Chava RK, Do JY, Kang M. Smart Hybridization of Au Coupled CdS Nanorods with Few Layered MoS2 Nanosheets for High Performance Photocatalytic Hydrogen Evolution Reaction. ACS Sustain Chem Eng 2018;6:6445–57. https://doi.org/10.1021/acssuschemeng.8b00249.

[79] Zhang M, Sun R, Li Y, Shi Q, Xie L, Chen J, et al. High H2 Evolution from Quantum Cu(II) Nanodot-Doped Two-Dimensional Ultrathin TiO2 Nanosheets with Dominant Exposed {001} Facets for Reforming Glycerol with Multiple Electron Transport Pathways. J Phys Chem C 2016;120:10746–56. https://doi.org/10.1021/acs.jpcc.6b01030.

[80] Xu Q, Zhu B, Jiang C, Cheng B, Yu J. Constructing 2D/2D Fe2O3/g-C3N4 Direct Z-Scheme Photocatalysts with Enhanced H2 Generation Performance. Sol RRL 2018;2:1800006. https://doi.org/10.1002/solr.201800006.

[81] Pavliuk M V., Fernandes AB, Abdellah M, Fernandes DLA, Machado CO, Rocha I, et al. Nano-hybrid plasmonic photocatalyst for hydrogen production at 20% efficiency. Sci Rep 2017;7:1–9. https://doi.org/10.1038/s41598-017-09261-7.

[82] Khon E, Lambright K, Khnayzer RS, Moroz P, Perera D, Butaeva E, et al. Improving the catalytic activity of semiconductor nanocrystals through selective domain etching. Nano Lett 2013;13:2016–23. https://doi.org/10.1021/nl400715n.

[83] Kalisman P, Nakibli Y, Amirav L. Perfect Photon-to-Hydrogen Conversion Efficiency. Nano Lett 2016;16:1776–81. https://doi.org/10.1021/acs.nanolett.5b04813.

[84] Moroz P, Boddy A, Zamkov M. Challenges and prospects of photocatalytic applications utilizing semiconductor nanocrystals. Front Chem 2018;6. https://doi.org/10.3389/fchem.2018.00353.

[85] Lu J, Zhang K, Liu XF, Zhang H, Sum TC, Neto AHC, et al. Order-disorder transition in a two-dimensional boron-carbon-nitride alloy. Nat Commun 2013;4:1–7. https://doi.org/10.1038/ncomms3681.

[86] Pati PB, Damas G, Tian L, Fernandes DLA, Zhang L, Pehlivan IB, et al. An experimental and theoretical study of an efficient polymer nano-photocatalyst for hydrogen evolution. Energy Environ Sci 2017;10:1372–6. https://doi.org/10.1039/c7ee00751e.

[87] Ye S, Wang R, Wu MZ, Yuan YP. A review on g-C 3 N 4 for photocatalytic water splitting and CO 2 reduction. Appl Surf Sci 2015;358:15–27. https://doi.org/10.1016/j.apsusc.2015.08.173.

[88] Kondarides DI, Daskalaki VM, Patsoura A, Verykios XE. Hydrogen production by photo-induced reforming of biomass components and derivatives at ambient conditions. Catal Letters 2008;122:26–32. https://doi.org/10.1007/s10562-007-9330-3.

[89] Anthony Raja M, Preethi V. Photocatalytic hydrogen production using bench-scale trapezoidal photocatalytic reactor. Int J Hydrogen Energy 2020;45:7574–83. https://doi.org/10.1016/j.ijhydene.2019.08.204.

[90] El-Maghrabi HH, Ali HR, Younis SA. Construction of a new ternary α-MoO3-WO3/CdS solar nanophotocatalyst towards clean water and hydrogen production from artificial wastewater using optimal design methodology. RSC Adv 2017;7:4409–21. https://doi.org/10.1039/c6ra25146c.

[91] Kaur K, Singh CV. Amorphous TiO2 as a photocatalyst for hydrogen production: A DFT study of structural and electronic properties. Energy Procedia 2012;29:291–9. https://doi.org/10.1016/j.egypro.2012.09.035.

[92] Hanaor DAH, Assadi MHN, Li S, Yu A, Sorrell CC. Ab initio study of phase stability in doped TiO2. Comput Mech 2012;50:185–94. https://doi.org/10.1007/s00466-012-0728-4.

[93] Das B, Choudhury B, Gomathi A, Manna AK, Pati SK, Rao CNR. Interaction of inorganic nanoparticles with graphene. ChemPhysChem 2011;12:937–43.

https://doi.org/10.1002/cphc.201001090.

[94] Kanda S, Akita T, Fujishima M, Tada H. Facile synthesis and catalytic activity of MoS2/TiO2 by a photodeposition-based technique and its oxidized derivative MoO3/TiO2 with a unique photochromism. J Colloid Interface Sci 2011;354:607–10. https://doi.org/10.1016/j.jcis.2010.11.007.

[95] Srivastava N, Srivastava M, Mishra PK, Kausar MA, Saeed M, Gupta VK, et al. Advances in nanomaterials induced biohydrogen production using waste biomass. Bioresour Technol 2020;307:123094. https://doi.org/10.1016/j.biortech.2020.123094.

[96] Lin R, Cheng J, Ding L, Song W, Liu M, Zhou J, et al. Enhanced dark hydrogen fermentation by addition of ferric oxide nanoparticles using Enterobacter aerogenes. Bioresour Technol 2016;207:213–9. https://doi.org/10.1016/j.biortech.2016.02.009.

[97] Taherdanak M, Zilouei H, Karimi K. Investigating the effects of iron and nickel nanoparticles on dark hydrogen fermentation from starch using central composite design. Int J Hydrogen Energy 2015;40:12956–63. https://doi.org/10.1016/j.ijhydene.2015.08.004.

[98] Ladole MR, Mevada JS, Pandit AB. Ultrasonic hyperactivation of cellulase immobilized on magnetic nanoparticles. Bioresour Technol 2017;239:117–26. https://doi.org/10.1016/j.biortech.2017.04.096.

[99] Srivastava N, Srivastava M, Manikanta A, Singh P, Ramteke PW, Mishra PK. Nanomaterials for biofuel production using lignocellulosic waste. Environ Chem Lett 2017;15:179–84. https://doi.org/10.1007/s10311-017-0622-6.

[100] Sambusiti C, Bellucci M, Zabaniotou A, Beneduce L, Monlau F. Algae as promising feedstocks for fermentative biohydrogen production according to a biorefinery approach: A comprehensive review. Renew Sustain Energy Rev 2015;44:20–36. https://doi.org/10.1016/j.rser.2014.12.013.

[101] Engliman NS, Abdul PM, Wu SY, Jahim JM. Influence of iron (II) oxide nanoparticle on biohydrogen production in thermophilic mixed fermentation. Int J Hydrogen Energy 2017;42:27482–93. https://doi.org/10.1016/j.ijhydene.2017.05.224.

[102] Wang J, Wan W. Influence of Ni2+ concentration on biohydrogen production. Bioresour Technol 2008;99:8864–8. https://doi.org/10.1016/j.biortech.2008.04.052.

[103] Han H, Cui M, Wei L, Yang H, Shen J. Enhancement effect of hematite nanoparticles on fermentative hydrogen production. Bioresour Technol 2011;102:7903–9. https://doi.org/10.1016/j.biortech.2011.05.089.

[104] Liu B, Jin Y, Wang Z, Xing D, Ma C, Ding J, et al. Enhanced photo-fermentative hydrogen production of Rhodopseudomonas sp. nov. strain A7 by the addition of TiO2, ZnO and SiC nanoparticles. Int J Hydrogen Energy 2017;42:18279–87. https://doi.org/10.1016/j.ijhydene.2017.04.147.

[105] Okolie JA, Mukherjee A, Nanda S, Dalai AK, Kozinski JA. Catalytic Supercritical Water Gasification of Soybean Straw: Effects of Catalyst Supports and Promoters. Ind Eng Chem Res 2021;60:5770–82. https://doi.org/10.1021/acs.iecr.0c06177.

[106] Norouzi O, Safari F, Jafarian S, Tavasoli A, Karimi A. Hydrothermal gasification performance of Enteromorpha intestinalis as an algal biomass for hydrogen-rich gas production using Ru promoted Fe–Ni/Γ-Al2O3 nanocatalysts. Energy Convers Manag 2017;141:63–71. https://doi.org/10.1016/j.enconman.2016.04.083.

[107] Velusamy K, Devanand J, Senthil Kumar P, Soundarajan K, Sivasubramanian V, Sindhu J, et al. A review on nano-catalysts and biochar-based catalysts for biofuel production. Fuel 2021;306:121632. https://doi.org/10.1016/j.fuel.2021.121632.

[108] Barati M, Babatabar M, Tavasoli A, Dalai AK, Das U. Hydrogen production via supercritical water gasification of bagasse using unpromoted and zinc promoted Ru/γ-Al2O3 nanocatalysts. Fuel Process Technol 2014;123:140–8. https://doi.org/10.1016/j.fuproc.2014.02.005.

[109] Rashidi M, Tavasoli A. Hydrogen rich gas production via supercritical water gasification of sugarcane bagasse using unpromoted and copper promoted Ni/CNT nanocatalysts. J Supercrit Fluids 2015;98:111–8. https://doi.org/10.1016/j.supflu.2015.01.008.

[110] Cao C, Xie Y, Mao L, Wei W, Shi J, Jin H. Hydrogen production from supercritical water gasification of soda black liquor with various metal oxides. Renew Energy 2020;157:24–32. https://doi.org/10.1016/j.renene.2020.04.143.

[111] Cao C, Zhang Y, Cao W, Jin H, Guo L, Huo Z. Transition Metal Oxides as Catalysts for Hydrogen Production from Supercritical Water Gasification of Glucose. Catal Letters 2017;147:828–36. https://doi.org/10.1007/s10562-017-2002-z.

[112] Nanda S, Reddy SN, Dalai AK, Kozinski JA. Subcritical and supercritical water gasification of lignocellulosic biomass impregnated with nickel nanocatalyst for hydrogen production. Int J Hydrogen Energy 2016;41:4907–21. https://doi.org/10.1016/j.ijhydene.2015.10.060.

[113] Kumar A, Reddy SN. Subcritical and supercritical water in-situ gasification of metal (Ni/Ru/Fe) impregnated banana pseudo-stem for hydrogen rich fuel gas mixture. Int J Hydrogen Energy 2020;45:18348–62. https://doi.org/10.1016/j.ijhydene.2019.08.009.

[114] Moradi R, Groth KM. Hydrogen storage and delivery: Review of the state of the art technologies and risk and reliability analysis. Int J Hydrogen Energy 2019;44:12254–69. https://doi.org/10.1016/j.ijhydene.2019.03.041.

[115] Rusman NAA, Dahari M. A review on the current progress of metal hydrides material for solid-state hydrogen storage applications. Int J Hydrogen Energy 2016;41:12108–26. https://doi.org/10.1016/j.ijhydene.2016.05.244.

[116] Zhevago NK, Chabak AF, Denisov EI, Glebov VI, Korobtsev S V. Storage of cryo-compressed hydrogen in flexible glass capillaries. Int J Hydrogen Energy 2013;38:6694–703. https://doi.org/10.1016/j.ijhydene.2013.03.107.

[117] Keçebaş A, Kayfeci M. Hydrogen properties. Sol. Hydrog. Prod. Process. Syst. Technol., Elsevier; 2019, p. 3–29. https://doi.org/10.1016/B978-0-12-814853-2.00001-1.

[118] Durbin DJ, Malardier-Jugroot C. Review of hydrogen storage techniques for on board vehicle applications. Int J Hydrogen Energy 2013;38:14595–617. https://doi.org/10.1016/j.ijhydene.2013.07.058.

[119] Peschel A. Industrial Perspective on Hydrogen Purification, Compression, Storage, and Distribution. Fuel Cells 2020;20:385–93. https://doi.org/10.1002/fuce.201900235.

[120] Berstad DO, Stang JH, Nekså P. Large-scale hydrogen liquefier utilising mixed-refrigerant pre-cooling. Int J Hydrogen Energy 2010;35:4512–23. https://doi.org/10.1016/j.ijhydene.2010.02.001.

[121] Tarhan C, Çil MA. A study on hydrogen, the clean energy of the future: Hydrogen storage methods. J Energy Storage 2021;40:102676. https://doi.org/10.1016/j.est.2021.102676.

[122] Elberry AM, Thakur J, Santasalo-Aarnio A, Larmi M. Large-scale compressed hydrogen storage as part of renewable electricity storage systems. Int J Hydrogen Energy 2021;46:15671–90. https://doi.org/10.1016/j.ijhydene.2021.02.080.

[123] Ozaki M, Tomura S, Ohmura R, Mori YH. Comparative study of large-scale hydrogen storage technologies: Is hydrate-based storage at advantage over existing technologies? Int J Hydrogen Energy 2014;39:3327–41. https://doi.org/10.1016/j.ijhydene.2013.12.080.

[124] Bossel U, Eliasson B. Energy and the Hydrogen Economy. ABB Switz Ltd 2009:1–35. https://afdc.energy.gov/files/pdfs/hyd_economy_bossel_eliasson.pdf; (accessed December 15, 2021).

[125] Niaz S, Manzoor T, Energy AP-R and S, 2015 U. Hydrogen storage: Materials, methods and perspectives. Elsevier 2015.

[126] Bracha M, Lorenz G, Patzelt A, Wanner M. Large-scale hydrogen liquefaction in Germany. Int J Hydrogen Energy 1994;19:53–9. https://doi.org/10.1016/0360-3199(94)90177-5.

[127] Kumar A, Raju NN, Muthukumar P, Selvan PV. Experimental studies on industrial scale metal hydride based hydrogen storage system with embedded cooling tubes. Int J Hydrogen Energy 2019;44:13549–60. https://doi.org/10.1016/j.ijhydene.2019.03.180.

[128] Chauhan PK, Parameshwaran R, Kannan P, Madhavaram R, Sujith R. Hydrogen storage in porous polymer derived SiliconOxycarbide ceramics: Outcomes and perspectives. Ceram Int 2021;47:2591–9. https://doi.org/10.1016/J.CERAMINT.2020.09.105.

[129] Souahlia A, Dhaou H, Mellouli S, Askri F, Jemni A, Ben Nasrallah S. Experimental study of metal hydride-based hydrogen storage tank at constant supply pressure. Int J Hydrogen Energy 2014;39:7365–72. https://doi.org/10.1016/j.ijhydene.2014.02.121.

[130] Cheng HM, Yang QH, Liu C. Hydrogen storage in carbon nanotubes. Carbon N Y 2001;39:1447–54. https://doi.org/10.1016/S0008-6223(00)00306-7.

[131] Li Y, Liu H. Grand canonical Monte Carlo simulation on the hydrogen storage behaviors of the cup-stacked carbon nanotubes at room temperature. Int J Hydrogen Energy 2021;46:6623–31. https://doi.org/10.1016/j.ijhydene.2020.11.139.

[132] Rather S ullah. Preparation, characterization and hydrogen storage studies of carbon nanotubes and their composites: A review. Int J Hydrogen Energy 2020;45:4653–72. https://doi.org/10.1016/j.ijhydene.2019.12.055.

[133] He H, Pham-Huy LA, Dramou P, Xiao D, Zuo P, Pham-Huy C. Carbon nanotubes: Applications in pharmacy and medicine. Biomed Res Int 2013;2013. https://doi.org/10.1155/2013/578290.

[134] Patel DK, Kim H, Dutta SD, Ganguly K, Lim K. Carbon Nanotubes-Based Nanomaterials and Their Agricultral and Biotechnological Applications. Materials (Basel) 2020:1–28.

[135] Mohan M, Sharma VK, Kumar EA, Gayathri V. Hydrogen storage in carbon materials-Areview. Energy Storage 2010:1–26. https://doi.org/10.1002/est2.35.

[136] Panella B, Hirscher M, Roth S. Hydrogen adsorption in different carbon nanostructures. Carbon N Y 2005;43:2209–14. https://doi.org/10.1016/j.carbon.2005.03.037.

[137] Park C, Keane MA. Controlled Growth of Highly Ordered Carbon Nanofibers from Y Zeolite Supported Nickel Catalysts. Langmuir 2001;17:8386–96.

[138] Li, X., Zhu, H., Ci, L., Xu, C., Mao, Z., Wei, B., et al. Hydrogen uptake by graphitized multi-walled carbon nanotubes under moderate pressure and at room temperature. Carbon N Y n.d.

[139] Tozzini V, Pellegrini V. Prospects for hydrogen storage in graphene. Phys Chem Chem Phys 2013;15:80–9. https://doi.org/10.1039/c2cp42538f.

[140] Dillon AC, Heben MJ. Hydrogen storage using carbon adsorbents : past , present and future. Appl Phys A 2001;72:133–42.

[141] Dillon AC, Jones KM, Bekkedahl TA, Kiang CH, Bethune DS, Heben MJ. Storage of hydrogen in single-walled carbon nanotubes. Nature 1997;386:377–9.

[142] Huang CW, Wu HC, Li YY. Hydrogen storage in platelet graphite nanofibers. Sep Purif Technol 2007;58:219–23. https://doi.org/10.1016/j.seppur.2007.07.032.

[143] Dillon AC., Jones KM., Bekkedahl TA., Klangt CH, Bethunet DS, Heben MJ. Storafe of hydrogen in single-walled carbon nanotubes. Lett to Nat 1997;668:1995–7.

[144] Yu X, Tang Z, Sun D, Ouyang L, Zhu M. Recent advances and remaining challenges of nanostructured materials for hydrogen storage applications. Prog Mater Sci 2017;88:1–48. https://doi.org/10.1016/j.pmatsci.2017.03.001.

[145] Ioannatos GE, Verykios XE. H2 storage on single- and multi-walled carbon nanotubes. Int J Hydrogen Energy 2010;35:622–8. https://doi.org/10.1016/j.ijhydene.2009.11.029.

[146] Shalabi AS, Abdel Halim WS, Abdel Aal S, Soliman KA. Tuning hydrogen storage of carbon nanotubes by mechanical bending: Theoretical study. Mol Simul 2016;42:709–14. https://doi.org/10.1080/08927022.2015.1085122.

[147] Srinivasan S, Demirocak DE, Kaushik A, Sharma M, Chaudhary GR, Hickman N, et al. Reversible hydrogen storage using nanocomposites. Appl Sci 2020;10. https://doi.org/10.3390/app10134618.

[148] Salehabadi A, Umar MF, Ahmad A, Ahmad MI, Ismail N, Rafatullah M. Carbon-based nanocomposites in solid-state hydrogen storage technology: An overview. Int J Energy Res 2020;44. https://doi.org/10.1002/er.5674.

[149] Yan Y, Au YS, Rentsch D, Remhof A, De Jongh PE, Züttel A. Reversible hydrogen storage in Mg(BH4)2/carbon nanocomposites. J Mater Chem A 2013;1. https://doi.org/10.1039/c3ta12222k.

[150] Ward PA, Teprovich JA, Peters B, Wheeler J, Compton RN, Zidan R. Reversible hydrogen storage in a LiBH4-C60 nanocomposite. J Phys Chem C 2013;117. https://doi.org/10.1021/jp4079103.

[151] Gross AF, Vajo JJ, Van Atta SL, Olson GL. Enhanced hydrogen storage kinetics of LiBH4 in nanoporous carbon scaffolds. J Phys Chem C 2008;112. https://doi.org/10.1021/jp711066t.

[152] Li L, Yao X, Sun C, Du A, Cheng L, Zhu Z, et al. Lithium-catalyzed dehydrogenation of ammonia borane within mesoporous carbon framework for chemical hydrogen storage. Adv Funct Mater 2009;19. https://doi.org/10.1002/adfm.200801111.

[153] Zhao-Karger Z, Witter R, Bardají EG, Wang D, Cossement D, Fichtner M. Altered reaction pathways of eutectic LiBH4-Mg(BH 4)2 by nanoconfinement. J Mater Chem A 2013;1. https://doi.org/10.1039/c2ta00542e.

[154] Gao J, Ngene P, Herrich M, Xia W, Gutfleisch O, Muhler M, et al. Interface effects in NaAlH4-carbon nanocomposites for hydrogen storage. Int J Hydrogen Energy 2014;39:10175–83. https://doi.org/10.1016/j.ijhydene.2014.03.188.

[155] Feaver A, Sepehri S, Shamberger P, Stowe A, Autrey T, Cao G. Coherent carbon cryogel-ammonia borane nanocomposites for H2 storage. J Phys Chem B 2007;111. https://doi.org/10.1021/jp072448t.

[156] Sepehri S, Garcia BB, Cao G. Tuning dehydrogenation temperature of carbon-ammonia borane nanocomposites. J Mater Chem 2008;18. https://doi.org/10.1039/b808511k.

[157] Figueroa-Torres MZ, Domínguez-Ríos C, Cabañas-Moreno JG, Vega-Becerra O, Aguilar-Elguézabal A. The synthesis of Ni-activated carbon nanocomposites via electroless deposition without a surface pretreatment as potential hydrogen storage materials. Int J Hydrogen Energy 2012;37. https://doi.org/10.1016/j.ijhydene.2012.04.097.

[158] Bravo Diaz L, Hanlon JM, Bielewski M, Milewska A, Gregory DH. Ammonia Borane Based Nanocomposites as Solid-State Hydrogen Stores for Portable Power Applications. Energy Technol 2018;6. https://doi.org/10.1002/ente.201700651.

[159] Zhu C, Chen M, Hu M, He D, Liu Y, Liu T. Hydrogen storage properties of Mg–Nb@C nanocomposite: Effects of Nb nanocatalyst and carbon nanoconfinement. Int J Hydrogen Energy 2021;46. https://doi.org/10.1016/j.ijhydene.2020.12.099.

[160] Liu Y, Zou J, Zeng X, Wu X, Tian H, Ding W, et al. Study on hydrogen storage properties of Mg nanoparticles confined in carbon aerogels. Int. J. Hydrogen Energy, vol. 38, 2013. https://doi.org/10.1016/j.ijhydene.2013.02.012.

[161] Cahen S, Eymery JB, Janot R, Tarascon JM. Improvement of the LiBH4 hydrogen desorption by inclusion into mesoporous carbons. J Power Sources 2009;189. https://doi.org/10.1016/j.jpowsour.2009.01.002.

[162] Mukherjee A, Okolie JA, Abdelrasoul A, Niu C, Dalai AK. Review of post-combustion carbon

dioxide capture technologies using activated carbon. J Environ Sci 2019;83:46–63. https://doi.org/10.1016/J.JES.2019.03.014.

[163] Strobel R, Garche J, Moseley PT, Wolf G, Institut F. Hydrogen storage by carbon materials. J Power Sources 2006;159:781–801. https://doi.org/10.1016/j.jpowsour.2006.03.047.

[164] Rajalakshmi N, Ramesh T. Activated Carbons-Promising Materials- Hydrogen Perspective. Agric Res Technol Open Access J 2017;10:1–3. https://doi.org/10.19080/ARTOAJ.2017.10.555776.

[165] Czarna-Juszkiewicz D, Cader J, Wdowin M. From coal ashes to solid sorbents for hydrogen storage. J Clean Prod 2020;270:122355. https://doi.org/10.1016/j.jclepro.2020.122355.

[166] Kapasiti P, Hidrogen P, Aktifan K. Hydrogen Adsorption Capacity Reduction of Activated Carbon Produced from Indonesia Low Rank Coal by Pelletizing. Sains Malays 2015;44:747–52.

[167] Zhao W, Luo L, Chen T, Li Z, Zhang Z, Fan M. Activated carbons from oil palm shell for hydrogen storage. IOP Conf. Ser. Mater. Sci. Eng., vol. 368, 2018, p. 368. https://doi.org/10.1088/1757-899X/368/1/012031.

[168] Akasaka H, Takahata T, Toda I, Ono H, Ohshio S. Hydrogen storage ability of porous carbon material fabricated from coffee bean wastes. Int J Hydrogen Energy 2010;36:580–5. https://doi.org/10.1016/j.ijhydene.2010.09.102.

[169] Fierro V, Szczurek A, Zlotea C, Mareche JF, Izquierdo MT, Albiniak A, et al. Experimental evidence of an upper limit for hydrogen storage at 77 K on activated carbons. Carbon N Y 2010;48:1902–11. https://doi.org/10.1016/j.carbon.2010.01.052.

[170] Alfadlil BR, Knowles GP, Parsa MR, Subagyono RRDJN, Daniel, Chaffee AL. Carbon monolith from Victorian brown coal for hydrogen storage. J Phys Conf Ser 2019;1277:1–7. https://doi.org/10.1088/1742-6596/1277/1/012024.

[171] Xu W, Takahashi K, Matsuo Y, Hattori Y, Kumagai M, Ishiyama S, et al. Investigation of hydrogen storage capacity of various carbon materials. Int J Hydrogen Energy 2007;32:2504–12. https://doi.org/10.1016/j.ijhydene.2006.11.012.

[172] Izquierdo MT, Celzard A. Impact of synthesis conditions of KOH activated carbons on their hydrogen storage capacities 2012;7:3–9. https://doi.org/10.1016/j.ijhydene.2012.06.110.

[173] Zhao W, Fierro V, Zlotea C, Izquierdo MT, Chevalier-César C, Latroche M, et al. Activated carbons doped with Pd nanoparticles for hydrogen storage. Int J Hydrogen Energy 2012;37:5072–80. https://doi.org/10.1016/j.ijhydene.2011.12.058.

[174] Orimo SI, Nakamori Y, Eliseo JR, Züttel A, Jensen CM. Complex hydrides for hydrogen storage. Chem Rev 2007;107:4111–32. https://doi.org/10.1021/cr0501846.

[175] He T, Cao H, Chen P. Complex Hydrides for Energy Storage, Conversion, and Utilization. Adv Mater 2019;31:1902757. https://doi.org/10.1002/adma.201902757.

[176] Møller KT, Sheppard D, Ravnsbæk DB, Buckley CE, Akiba E, Li HW, et al. Complex metal hydrides for hydrogen, thermal and electrochemical energy storage. Energies 2017;10:1645. https://doi.org/10.3390/en10101645.

[177] Andersson J, Grönkvist S. Large-scale storage of hydrogen. Int J Hydrogen Energy 2019;44:11901–19. https://doi.org/10.1016/j.ijhydene.2019.03.063.

[178] Ley MB, Jepsen LH, Lee YS, Cho YW, Bellosta Von Colbe JM, Dornheim M, et al. Complex hydrides for hydrogen storage - New perspectives. Mater Today 2014;17:122–8. https://doi.org/10.1016/j.mattod.2014.02.013.

[179] Gupta A, Baron G V., Perreault P, Lenaerts S, Ciocarlan RG, Cool P, et al. Hydrogen Clathrates: Next Generation Hydrogen Storage Materials. Energy Storage Mater 2021;41:69–107. https://doi.org/10.1016/j.ensm.2021.05.044.

[180] Luo Y, Wang Q, Li J, Xu F, Sun L, Zou Y, et al. Enhanced hydrogen storage/sensing of metal hydrides by nanomodification. Mater Today Nano 2020;9:100071. https://doi.org/10.1016/j.mtnano.2019.100071.

[181] Zhang X, Ren Z, Zhang X, Gao M, Pan H, Liu Y. Triggering highly stable catalytic activity of metallic titanium for hydrogen storage in NaAlH 4 by preparing ultrafine nanoparticles. J Mater Chem A 2019;7:4651–9. https://doi.org/10.1039/c9ta00748b.

[182] Santoru A, Pistidda C, Brighi M, Chierotti MR, Heere M, Karimi F, et al. Insights into the Rb-Mg-N-H System: An Ordered Mixed Amide/Imide Phase and a Disordered Amide/Hydride Solid Solution. Inorg Chem 2018;57:3197–205. https://doi.org/10.1021/acs.inorgchem.7b03232.

[183] Pohlmann C, Röntzsch L, Hu J, Weißgärber T, Kieback B, Fichtner M. Tailored heat transfer characteristics of pelletized LiNH 2-MgH 2 and NaAlH 4 hydrogen storage materials. J Power Sources 2012;205:173–9. https://doi.org/10.1016/j.jpowsour.2012.01.064.

[184] Milanese C, Garroni S, Gennari F, Marini A, Klassen T, Dornheim M, et al. Solid state hydrogen storage in alanates and alanate-based compounds: A review. Metals (Basel) 2018;8:567. https://doi.org/10.3390/met8080567.

[185] Fan X, Xiao X, Chen L, Zhang L, Shao J, Li S, et al. Significantly improved hydrogen storage properties of NaAlH4 catalyzed by Ce-based nanoparticles. J Mater Chem A 2013;1:9752–9. https://doi.org/10.1039/c3ta11860f.

[186] Baldé CP, Hereijgers BPC, Bitter JH, De Jong KP. Sodium alanate nanoparticles - Linking size to hydrogen storage properties. J Am Chem Soc 2008;130:6761–5. https://doi.org/10.1021/ja710667v.

[187] Zheng S, Fang F, Zhou G, Chen G, Ouyang L, Zhu M, et al. Hydrogen storage properties of space-confined NaAlH4 nanoparticles in ordered mesoporous silica. Chem Mater 2008;20:3954–8. https://doi.org/10.1021/cm8002063.

[188] Liu Y, Zhang X, Wang K, Yang Y, Gao M, Pan H. Achieving ambient temperature hydrogen storage in ultrafine nanocrystalline TiO2@C-doped NaAlH4. J Mater Chem A 2016;4:1087–95. https://doi.org/10.1039/c5ta09400c.

[189] Zhang X, Ren Z, Lu Y, Yao J, Gao M, Liu Y, et al. Facile Synthesis and Superior Catalytic Activity of Nano-TiN@N-C for Hydrogen Storage in NaAlH4. ACS Appl Mater Interfaces 2018;10:15767–77. https://doi.org/10.1021/acsami.8b04011.

[190] Li L, Qiu F, Wang Y, Liu G, Xu Y, An C, et al. TiN catalyst for the reversible hydrogen storage performance of sodium alanate system. J Mater Chem 2012;22:13782–7. https://doi.org/10.1039/c2jm31388j.

[191] Arora E, Saini S, Basera P, Kumar M, Singh A, Bhattacharya S. Elucidating the Role of Temperature and Pressure to the Thermodynamic Stability of Charged Defects in Complex Metal-Hydrides: A Case Study of NaAlH 4. J Phys Chem C 2019;123:62–9. https://doi.org/10.1021/acs.jpcc.8b08687.

[192] Kang SY, Heo TW, Allendorf MD, Wood BC. Morphology-Dependent Stability of Complex Metal Hydrides and Their Intermediates Using First-Principles Calculations. ChemPhysChem 2019;20:1340–7. https://doi.org/10.1002/cphc.201801132.

[193] Züttel A, Borgschulte A, Orimo SI. Tetrahydroborates as new hydrogen storage materials. Scr Mater 2007;56:823–8. https://doi.org/10.1016/j.scriptamat.2007.01.010.

[194] Lai Q, Aguey-Zinsou KF. Destabilisation of Ca(BH4)2 and Mg(BH4)2: Via confinement in nanoporous Cu2S hollow spheres. Sustain Energy Fuels 2017;1:1308–19. https://doi.org/10.1039/c7se00121e.

[195] Huang Z, Wang Y, Wang D, Yang F, Wu Z, Zhang Z. Influence of transition metals Fe, Co, Ni, Cu and Ti on the dehydrogenation characteristics of LiBH4: A first-principles investigation. Comput Theor Chem 2018;1133:33–9. https://doi.org/10.1016/j.comptc.2018.04.017.

[196] Chen P, Xiong Z, Luo J, Lin J, Lee Tan K. Interaction of hydrogen with metal nitrides and imides. Nature 2002;420:302–4. https://doi.org/10.1038/nature01210.

[197] Wood BC, Heo TW, Kang S, Wan LF, Li S. Beyond Idealized Models of Nanoscale Metal Hydrides for Hydrogen Storage. Ind Eng Chem Res 2020;59:5786–96. https://doi.org/10.1021/acs.iecr.9b06617.

[198] Cao H, Pistidda C, Richter TMM, Santoru A, Milanese C, Garroni S, et al. In situ x-ray diffraction studies on the de/rehydrogenation processes of the K2[Zn(NH 2)4]-8LiH system. J Phys Chem C 2017;121:1546–51. https://doi.org/10.1021/acs.jpcc.6b12095.

[199] Shaw LL, Ren R, Markmaitree T, Osborn W. Effects of mechanical activation on dehydrogenation of the lithium amide and lithium hydride system. J Alloys Compd 2008;448:263–71. https://doi.org/10.1016/j.jallcom.2006.10.029.

[200] Zhou HCJ, Kitagawa S. Metal-Organic Frameworks (MOFs). Chem Soc Rev 2014;43:5415–8. https://doi.org/10.1039/c4cs90059f.

[201] Janiak C. Engineering coordination polymers towards applications. J Chem Soc Dalt Trans 2003;3:2781–804. https://doi.org/10.1039/b305705b.

[202] Zeleňák V, Saldan I. Factors affecting hydrogen adsorption in metal–organic frameworks: A short review. Nanomaterials 2021;11:1638. https://doi.org/10.3390/nano11071638.

[203] Lin X, Jia J, Champness NR, Hubberstey P, Schröder M. Metal-organic framework materials for hydrogen storage. Solid-State Hydrog Storage Mater Chem 2008:288–312. https://doi.org/10.1533/9781845694944.3.288.

[204] Sule R, Mishra AK, Nkambule TT. Recent advancement in consolidation of MOFs as absorbents for hydrogen storage. Int J Energy Res 2021;45:12481–99. https://doi.org/10.1002/er.6608.

[205] Ockwig NW, Delgado-Friedrichs O, O'Keeffe M, Yaghi OM. Reticular chemistry: Occurrence and taxonomy of nets and grammar for the design of frameworks. Acc Chem Res 2005;38:176–82. https://doi.org/10.1021/ar020022l.

[206] U.S Deparment of Energy. DOE Technical Targets for Onboard Hydrogen Storage for Light-Duty Vehicles | Department of Energy. EnergyGov 2017:1–23. https://www.energy.gov/eere/fuelcells/doe-technical-targets-onboard-hydrogen-storage-light-duty-vehicles%0Ahttps://energy.gov/eere/fuelcells/doe-technical-targets-onboard-hydrogen-storage-light-duty-vehicles (accessed September 1, 2021).

[207] Ahmed A, Liu Y, Purewal J, Tran LD, Wong-Foy AG, Veenstra M, et al. Balancing gravimetric and volumetric hydrogen density in MOFs. Energy Environ Sci 2017;10:2459–71. https://doi.org/10.1039/c7ee02477k.

[208] Collins DJ, Zhou HC. Hydrogen storage in metal-organic frameworks. J Mater Chem 2007;17:3154–60. https://doi.org/10.1039/b702858j.

[209] Yaghi OM, O'Keeffe M, Ockwig NW, Chae HK, Eddaoudi M, Kim J. Reticular synthesis and the design of new materials. Nature 2003;423:705–14. https://doi.org/10.1038/nature01650.

[210] Koh K, Wong-Foy AG, Matzger AJ. A porous coordination copolymer with over 5000 m 2/g BET surface area. J Am Chem Soc 2009;131:4184–5. https://doi.org/10.1021/ja809985t.

[211] Klein N, Senkovska I, Gedrich K, Stoeck U, Henschel A, Mueller U, et al. A mesoporous metal-organic framework. Angew Chemie - Int Ed 2009;48:9954–7. https://doi.org/10.1002/anie.200904599.

[212] Deng H, Doonan CJ, Furukawa H, Ferreira RB, Towne J, Knobler CB, et al. Multiple functional groups of varying ratios in metal-organic frameworks. Science (80- ) 2010;327:846–50. https://doi.org/10.1126/science.1181761.

[213] Ma L, Jin A, Xie Z, Lin W. Freeze drying significantly increases permanent porosity and hydrogen uptake in 4,4-connected metal-organic frameworks. Angew Chemie - Int Ed 2009;48:9905–8. https://doi.org/10.1002/anie.200904983.

[214] Cooper AI, Rosseinsky MJ. Metal-organic frameworks: Improving pore performance. Nat Chem 2009;1:26–7. https://doi.org/10.1038/nchem.157.

[215] Xiang Z, Cao D, Shao X, Wang W, Zhang J, Wu W. Facile preparation of high-capacity hydrogen storage metal-organic frameworks: A combination of microwave-assisted solvothermal synthesis and supercritical activation. Chem Eng Sci 2010;65:3140–6. https://doi.org/10.1016/J.CES.2010.02.005.

[216] Zhou W, Wu H, Yildirim T. Enhanced H2 adsorption in isostructural metal-organic frameworks with open metal sites: Strong dependence of the binding strength on metal ions. J Am Chem Soc 2008;130:15268–9. https://doi.org/10.1021/ja807023q.

[217] Bagheri M, Masoomi MY, Domínguez E, García H. High hydrogen release catalytic activity by

quasi-MOFs prepared via post-synthetic pore engineering . Sustain Energy Fuels 2021. https://doi.org/10.1039/d1se00661d.

[218] Rowsell JLC, Millward AR, Park KS, Yaghi OM. Hydrogen Sorption in Functionalized Metal-Organic Frameworks. J Am Chem Soc 2004;126:5666–7. https://doi.org/10.1021/ja049408c.

[219] Mavrandonakis A, Tylianakis E, Stubos AK, Froudakis GE. Why Li doping in MOFs enhances H2 storage capacity? A multi-scale theoretical study. J Phys Chem C 2008;112:7290–4. https://doi.org/10.1021/jp7102098.

[220] Cheng H, Chen L, Cooper AC, Sha X, Pez GP. Hydrogen spillover in the context of hydrogen storage using solid-state materials. Energy Environ Sci 2008;1:338–54. https://doi.org/10.1039/b807618a.

[221] Suresh K, Aulakh D, Purewal J, Siegel DJ, Veenstra M, Matzger AJ. Optimizing Hydrogen Storage in MOFs through Engineering of Crystal Morphology and Control of Crystal Size. J Am Chem Soc 2021;143:10727–34. https://doi.org/10.1021/jacs.1c04926.

[222] Kolotilov S V., Pavlishchuk V V. Effect of structural and thermodynamic factors on the sorption of hydrogen by metal-organic framework compounds. Theor Exp Chem 2009;45:75–97. https://doi.org/10.1007/s11237-009-9068-7.

[223] Mao WL, Mao H. Hydrogen storage in molecular compounds. Proc Natl Acad Sci 2004;101:708–10. https://doi.org/10.1073/PNAS.0307449100.

[224] Struzhkin V V., Militzer B, Mao WL, Mao HK, Hemley RJ. Hydrogen storage in molecular clathrates. Chem Rev 2007;107:4133–51. https://doi.org/10.1021/cr050183d.

[225] Chattaraj PK, Bandaru S, Mondal S. Hydrogen storage in clathrate hydrates. J Phys Chem A 2011;115:187–93. https://doi.org/10.1021/jp109515a.

[226] Mao WL, Mao H kwang, Goncharov AF, Struzhkin V V., Guo Q, Hu J, et al. Hydrogen clusters in clathrate hydrate. Science (80- ) 2002;297:2247–9. https://doi.org/10.1126/science.1075394.

[227] Florusse LJ, Peters CJ, Schoonman J, Hester KC, Koh CA, Dec SF, et al. Stable low-pressure hydrogen clusters stored in a binary clathrate hydrate. Science (80- ) 2004;306:469–71. https://doi.org/10.1126/science.1102076.

[228] Du JW, Liang DQ, Dai XX, Li DL, Li XJ. Hydrate phase equilibrium for the (hydrogen + tert-butylamine + water) system. J Chem Thermodyn 2011;43:617–21. https://doi.org/10.1016/j.jct.2010.11.018.

[229] Du J, Wang L, Liang D, Li D. Phase equilibria and dissociation enthalpies of hydrogen semi-clathrate hydrate with tetrabutyl ammonium nitrate. J Chem Eng Data 2012;57:603–9. https://doi.org/10.1021/je201177t.

[230] Cai J, Tao YQ, von Solms N, Xu CG, Chen ZY, Li X Sen. Experimental studies on hydrogen hydrate with tetrahydrofuran by differential scanning calorimeter and in-situ Raman. Appl Energy 2019;243:1–9. https://doi.org/10.1016/j.apenergy.2019.03.179.

[231] Liu J, Hou J, Xu J, Liu H, Chen G, Zhang J. Ab initio study of the molecular hydrogen occupancy in

pure H2 and binary H2-THF clathrate hydrates. Int J Hydrogen Energy 2017;42:17136–43. https://doi.org/10.1016/j.ijhydene.2017.06.025.

[232] Ghaani MR, Takeya S, English NJ. Hydrogen storage in propane-hydrate: Theoretical and experimental study. Appl Sci 2020;10:1–10. https://doi.org/10.3390/app10248962.

[233] Zhang Y, Bhattacharjee G, Zheng J, Linga P. Hydrogen storage as clathrate hydrates in the presence of 1,3-dioxolane as a dual-function promoter. Chem Eng J 2022;427:131771. https://doi.org/10.1016/j.cej.2021.131771.

[234] Prasad PSR, Sugahara T, Sum AK, Sloan ED, Koh CA. Hydrogen storage in double clathrates with tert-butylamine. J Phys Chem A 2009;113:6540–3. https://doi.org/10.1021/jp9029997.

[235] Amano S, Tsuda T, Hashimoto S, Sugahara T, Ohgaki K. Competitive cage occupancy of hydrogen and argon in structure-II hydrates. Fluid Phase Equilib 2010;298:113–6. https://doi.org/10.1016/j.fluid.2010.07.017.

[236] Lu H, Wang J, Liu C, Ratcliffe CI, Becker U, Kumar R, et al. Multiple H 2 occupancy of cages of clathrate hydrate under mild conditions. J Am Chem Soc 2012;134:9160–2. https://doi.org/10.1021/ja303222u.

[237] Lee S, Lee Y, Park S, Kim Y, Lee JD, Seo Y. Thermodynamic and spectroscopic identification of guest gas enclathration in the double tetra-n-butylammonium fluoride semiclathrates. J Phys Chem B 2012;116:9075–81. https://doi.org/10.1021/jp302647c.

[238] Matsumoto M, Tanaka H. On the structure selectivity of clathrate hydrates. J Phys Chem B 2011;115:8257–65. https://doi.org/10.1021/jp203478z.

[239] Lee BR, Sa JH, Hong SY, Lee JD, Lee KH, Seo Y, et al. Guest-Guest Interactions and Co-Occupation by Distinct Guests in the Metastable State of Clathrate Hydrates. J Phys Chem C 2019;123:3811–6. https://doi.org/10.1021/acs.jpcc.8b08629.

[240] Del Rosso L, Celli M, Ulivi L. Raman Measurements of Pure Hydrogen Clathrate Formation from a Supercooled Hydrogen-Water Solution. J Phys Chem Lett 2015;6:4309–13. https://doi.org/10.1021/acs.jpclett.5b01923.

[241] Veluswamy HP, Yew JC, Linga P. New hydrate phase equilibrium data for two binary gas mixtures of hydrogen and propane coupled with a kinetic study. J Chem Eng Data 2015;60:228–37. https://doi.org/10.1021/je500489d.

[242] Veluswamy HP, Linga P. Macroscopic kinetics of hydrate formation of mixed hydrates of hydrogen/tetrahydrofuran for hydrogen storage. Int J Hydrogen Energy 2013;38:4587–96. https://doi.org/10.1016/j.ijhydene.2013.01.123.

[243] Veluswamy HP, Chen JY, Linga P. Surfactant effect on the kinetics of mixed hydrogen/propane hydrate formation for hydrogen storage as clathrates. Chem Eng Sci 2015;126:488–99. https://doi.org/10.1016/j.ces.2014.12.052.

[244] Di Profio P, Canale V, Germani R, Arca S, Fontana A. Reverse micelles enhance the formation of clathrate hydrates of hydrogen. J Colloid Interface Sci 2018;516:224–31. https://doi.org/10.1016/j.jcis.2018.01.059.

[245] Oshima M, Shimada W, Hashimoto S, Tani A, Ohgaki K. Memory effect on semi-clathrate hydrate formation: A case study of tetragonal tetra-n-butyl ammonium bromide hydrate. Chem Eng Sci 2010;65:5442–6. https://doi.org/10.1016/j.ces.2010.07.019.

[246] Zhao J, Wang C, Yang M, Liu W, Xu K, Liu Y, et al. Existence of a memory effect between hydrates with different structures (I, II, and H). J Nat Gas Sci Eng 2015;26:330–5. https://doi.org/10.1016/j.jngse.2015.06.031.

[247] Lan R, Irvine JTS, Tao S. Ammonia and related chemicals as potential indirect hydrogen storage materials. Int J Hydrogen Energy 2012;37:1482–94. https://doi.org/10.1016/j.ijhydene.2011.10.004.

[248] McKinlay CJ, Turnock SR, Hudson DA. Route to zero emission shipping: Hydrogen, ammonia or methanol? Int J Hydrogen Energy 2021;46:28282–97. https://doi.org/10.1016/j.ijhydene.2021.06.066.

[249] Aziz M, TriWijayanta A, Nandiyanto ABD. Ammonia as effective hydrogen storage: A review on production, storage and utilization. Energies 2020;13:3062. https://doi.org/10.3390/en13123062.